CLM - R 169

CLM - R 169

UKAEA

Report

APPLICATIONS OF LABORATORY AND THEORETICAL MHD DUCT FLOW STUDIES IN FUSION REACTOR TECHNOLOGY

J C R HUNT
R J HOLROYD

CULHAM LABORATORY
Abingdon Oxfordshire

1977

Available from H. M. Stationery Office

C/18

£1.50

CLM-R169

APPLICATIONS OF LABORATORY AND THEORETICAL MHD DUCT FLOW STUDIES IN FUSION REACTOR TECHNOLOGY

J.C.R. Hunt , R.J. Holroyd

Dept. of Engineering, Univ. of Cambridge

ABSTRACT

The great advances in MHD duct flow studies, both theoretical and experimental, during the past few years have left earlier estimates of the pumping power required to circulate the liquid lithium coolant through the blanket of a nuclear fusion reactor out of date. This report attempts to collate recent MHD research studies relevant to fusion reactor technology. It is shown that non-uniform magnetic fields and area changes of the pipes containing the coolant flow can dramatically alter the flows found when the field is uniform and the pipe straight by distorting the velocity profile, increasing pressure gradients and introducing large pressure drops into the system. In some situations the flow can even be confined to extremely thin layers parallel to the magnetic field lines. Such effects could have a detrimental effect on the heat transfer properties of the coolant and may necessitate radical changes in the designs for some parts of the blanket.

Culham Laboratory
Euratom/UKAEA Fusion Association
Abingdon
Oxfordshire

May 1977

SBN 85311 053 0

CONTENTS

1. INTRODUCTION

1.1 Aim and scope of the report

If magnetic confinement fusion reactors are to be cooled by liquid metals then the flow of the coolant through the pipework in the magnetic field will inevitably be very complicated, involving, for example, flows in non-uniform magnetic fields, in pipes with changing cross-section, annular pipe flow, flows between baffles set in pipes and flows at junctions of pipes. Previous estimates of the pressure required to pump the liquid metal coolant were mainly based on the known pressure losses of straight pipes situated in uniform magnetic fields (e.g. Hunt & Hancox[1]). However, it was realised then that these estimates could be seriously in error because of the neglect of the complexities of real cooling circuits.

This report summarises the theoretical and experimental studies of the flow of liquid metals along pipes situated in strong magnetic fields that have been made during the past six years or so. We emphasise the work that we have done at Cambridge with the support of the U.K.A.E.A. and, latterly, S.R.C., but we also review the work done elsewhere, notably the theoretical work of Walker and Ludford at the Universities of Illinois and Cornell and of Kulikovskii at Moscow University, and the experimental work of Carlson at Livermore and of Fraas at Oak Ridge.

These recent studies have concentrated particularly on the complexities likely to occur in real coolant circuits. We show that if the pipe walls are electrically insulating or, if electrically conducting are so thin that their conductance is much less than that of the liquid metal, then the broad patterns of the flow in regions of varying magnetic field strength or duct cross-sectional area can be predicted quite simply by plotting the paths of 'characteristic surfaces' which are a function of both the shape of the duct and the magnetic field. This principle is explained in sec.2.2 and the concept is applied to flows in different types of duct in secs. 3.1, 3.2 and 3.3. Sec.3.4 looks at flows in highly conducting walled ducts and flows in rectangular ducts are discussed in secs.3.5 and 3.6.

In sec.4.2 we describe our experimental facility for studying the flow of mercury along several uniform bore ducts, each having walls of different electrical conductivity, situated in transverse, non-uniform magnetic fields. Our measurements of pressures and velocities are compared with the theoretical predictions in secs. 4.3-4.6 and 5. Comparisons are made with liquid metal MHD experiments carried out elsewhere; on the whole our experiments appear to be unique in that there have been no other systematic measurements of MHD duct flows in strong, non-uniform, transverse magnetic fields.

Finally, after a short discussion on entry lengths in sec.6, in sec.7 we examine and discuss some aspects of recent designs for fusion reactor blankets in the context of our findings.

1.2 Typical parameters for MHD duct flows in a fusion reactor

The typical parameters for the flow of liquid metals in the cooling circuit were set out in the aforementioned report[1]. They are

$$M = \text{Hartmann number} \approx \left(\frac{\text{electromagnetic stresses}}{\text{viscous stresses}}\right)^{\frac{1}{2}} = aB_o\left(\frac{\sigma}{\eta}\right)^{\frac{1}{2}} \approx 35000$$

$$R_e = \text{Reynolds number} \approx \frac{\text{viscous stresses}}{\text{inertial stresses}} = \frac{av_o\rho}{\eta} \approx 28000$$

$$N = \text{interaction parameter} \approx \frac{\text{electromagnetic stresses}}{\text{inertial stresses}} = \frac{M^2}{R_e} = \frac{\sigma B_o^2 a}{\rho v_o} \approx 44000$$

$$R_m = \text{magnetic Reynolds number} \approx \frac{\text{induced magnetic field strength}}{\text{imposed magnetic field strength}} = \sigma_o v\mu a \approx 0.07$$

Here B_o, v_o and a are typical values of magnetic flux density (10 T), mean velocity (0.5 m/s) and hydraulic radius of the pipe (0.05m) respectively while σ, η, ρ and μ represent the electrical conductivity, viscosity, density and magnetic permeability of the liquid metal, namely lithium.

Since the pressure gradients increase as the conductance of the duct walls increases then ideally duct walls should be non-conducting[1]. Unfortunately, at the high temperatures which will be found in a fusion reactor, say 500°C, non-conducting materials which are strong enough to contain liquid metals at high pressure do not exist and so metallic pipework with electrical conductivity σ_w and wall thickness t will be employed. To reduce the conductance of the wall and to avoid waste of neutrons from the plasma, t/a must be as small as possible subject to the requirement that the pipe be strong enough to withstand the pressure loading. Calculations by Hancox & Booth[2] point to $t/a < 0.1$ for stainless steel pipes. Thus, for the flow of liquid lithium in such pipes the conductance ratio $\phi = \sigma_w t/\sigma a$, which is the non-dimensional parameter representing the ratio of the conductance of the wall to that of the fluid, will have a value in the range 0.05-0.1. Hoffman & Carlson[3] suggest $\phi < 0.01$ for lithium in niobium pipes. However, their value of $t/a \approx 0.01$ is calculated on the basis of an idealised flow circuit which might be very difficult to realise in practice.

2. REVIEW OF MHD DUCT FLOW THEORY WHEN M >> 1

2.1 Governing equations and assumptions

The derivation of the MHD equations for a fluid with constant properties is given, for example, by Shercliff[4]. In non-dimensional form they are

$$\frac{\partial \underline{v}'}{\partial \tau'} + \underline{v}'.\nabla\underline{v}' = -\nabla p' + N\underline{j}' \wedge \underline{B}' + R_e^{-1}\nabla^2\underline{v}' \qquad (2.1a)$$

$$\nabla.\underline{v}' = 0 \qquad \underline{j}' = \underline{E}' + \underline{v}' \wedge \underline{B}' \qquad \nabla.\underline{j}' = 0 \qquad (2.1b,c,d)$$

$$\partial\underline{B}'/\partial\tau' = -\nabla \wedge \underline{E}' \qquad \underline{j}' = R_m^{-1}\nabla \wedge \underline{B}' \qquad \nabla.\underline{B}' = 0 \qquad (2.1e,f,g)$$

where $\underline{v}'$, $\underline{j}'$, $\underline{B}'$, $\underline{E}'$, p' and τ' represent the non-dimensional variables velocity, current density, magnetic field strength, electric field strength, pressure

and time respectively. The corresponding physical quantities, which are represented by the same character but without the dash, are related to their non-dimensional counterparts by

$$\underline{v} = v_o \underline{v}' \qquad \underline{j} = \sigma v_o B_o \underline{j}' \qquad \underline{B} = B_o \underline{B}'$$

$$\underline{E} = v_o B_o \underline{E}' \qquad p = \rho v_o^2 p' \qquad \tau = (a/v_o)\tau'$$

Since N and R_e are so large in typical reactor pipework, we can look for asymptotic solutions to equations (2.1) in the limits $N \to \infty$ and $R_e \to \infty$. In that case equation (2.1a) reduces to

$$-\nabla(p'/N) + \underline{j}' \wedge \underline{B}' = 0 \qquad (2.2a)$$

or, by taking the curl of it

$$\nabla \wedge (\underline{j}' \wedge \underline{B}') \equiv (\underline{B}'.\nabla)\underline{j}' - (\underline{j}'.\nabla)\underline{B}' = 0$$

This approximation only breaks down in

(i) boundary layers of thickness $O(aM^{-1})$ adjacent to walls which cut magnetic field lines (see sec.2.2)

(ii) shear layers of thickness $O(aM^{-\frac{1}{2}})$ parallel to both the field lines and the mean flow (see sec.2.6)

(iii) layers of maximum thickness $O(aN^{-1/3})$ within the flow parallel to the field lines but not the mean flow (see sec. 2.6)

(iv) regions of width $O(aM^{-2/3}) \times O(aM^{-1/3})$ where field lines are tangential to a curved pipe wall (see Roberts[5])

Regions where equation (2.2a) holds, which includes most of the flow, are usually called 'core flow' regions and are denoted by 'C' in Figs.1a,b.

If the applied magnetic field is steady (as it would be in some kinds of fusion reactor), $\partial \underline{B}'/\partial\tau' \equiv 0$ and equation (2.1e) shows that the electric field is irrotational. Accordingly, $\underline{E}'$ can be expressed in terms of an electric potential Φ' $(= \Phi/av_oB_o)$ as $\underline{E}' = -\nabla\Phi'$. Noting that $R_m \ll 1$ (sec.1.2), equations (2.1b-g) may now be rewritten as

$$\nabla.\underline{v}' = 0 \qquad \underline{j}' = -\nabla\Phi' + \underline{v}' \wedge \underline{B}' \qquad (2.2b,c)$$

$$\nabla.\underline{j}' = 0 \qquad \nabla \wedge \underline{B}' = \nabla.\underline{B}' = 0 \qquad (2.2d,e,f)$$

Equations (2.2e,f) allow $\underline{B}'$ to be defined in terms of a magnetic vector potential $\underline{A}$ and a magnetic scalar potential ψ as

$$\underline{B}' = \nabla \wedge \underline{A}' = \nabla\psi \qquad (2.2g,h)$$

so that magnetic field lines are defined by lines along which $\underline{A}$ = constant.

A general solution to equations (2.2) for $\underline{v}'$, $\underline{j}'$ and Φ' was deduced by Kulikovskii[6] in the form of integrals of $\underline{B}'$, $\nabla p'$ and their derivatives along the magnetic field lines together with four unknown functions, one being p', which are determined by the boundary conditions (see Appendix I). It follows that the boundary layers which primarily determine the core flow are those on the walls which cut the field lines (see Fig.2 and sec.2.2). Depending on the value

of ϕ, the changes in $\underline{v}'$, $\underline{j}'$ and Φ' across such boundary layers vary enormously. However, we will show that if the value of ϕ lies in one of three ranges, namely $\phi << M^{-1}$, $M^{-1} << \phi << 1$ and $\phi >> 1$, then different terms in Kulikovskii's general solution can be neglected thus enabling particular solutions to be found in a fairly straightforward manner.

One important implication of Kulikovskii's solution is that given finite, steady values of the flow variables at the boundaries of the core flow region, then no instabilities can be generated in the core region. In other words, if the boundary and shear layers are stable then the whole flow is stable and no turbulence can develop.

2.2 Hartmann layers

Boundary layers in which there is a significant component of $\underline{B}$ normal to the wall are known as Hartmann layers and are labelled 'H' in Fig.1a. For $N >> 1$ the inertial term $\underline{v}'.\nabla\underline{v}'$ can be neglected in equation (2.1a) and the resulting boundary layer equations are readily solved (Kulikovskii[6], Hunt & Ludford[7]). In terms of the dimensionless normal co-ordinate to the wall directed into the fluid, $\underline{n}'$, and the associated unit vector $\hat{n} = \underline{n}'/|\underline{n}'|$ (see Fig.2), the velocity and current density distributions in the layer are given by

$$\underline{v}' = \underline{v}'_\infty \{1 - \exp(-M|\underline{n}'.\underline{B}'|)\} \qquad (2.3a)$$

$$\underline{j}' \wedge \hat{n} = \underline{j}'_\infty \wedge \hat{n} - (\underline{v}'_\infty \wedge \underline{B}') \wedge \hat{n} \exp(-M|\underline{n}'.\underline{B}'|) \qquad (2.3b)$$

where $\underline{v}'_\infty$ and $\underline{j}'_\infty$ denote the core flow values of those quantities outside the layer as $n' \to \infty$. Since $\underline{v}' \equiv 0$ on the wall, the component of the core velocity normal to the wall is very small; i.e.

$$\underline{v}'_\infty.\hat{n} = O(M^{-1}) \quad \text{as} \quad n' \to 0 \qquad (2.4)$$

Note that the thickness of these Hartmann layers is inversely proportional to the component normal to the wall of the local value of $\underline{B}'$. The values of $\underline{j}'$ and Φ' in these layers also depend on the electrical properties of the wall as will be shown in secs.2.3, 2.4 and 2.5.

2.3 Ducts with non-conducting walls ($\phi << M^{-1}$)

At such a wall the electrical boundary condition is

$$\underline{j}'.\hat{n} = \partial\Phi'/\partial n' \equiv 0 \quad \text{at} \quad n' = 0 \qquad (2.5)$$

Thence, by applying the equation of current continuity (2.2d) to equation (2.3b) it follows that for a continuously curving surface

$$\underline{j}'_\infty.\hat{n} = \text{sign}(\hat{n}.\underline{B}')M^{-1}(\nabla \wedge \underline{v}')_\infty.\hat{n} \qquad (2.6)$$

or, for a general surface $\underline{j}'_\infty.\hat{n} = O(M^{-1})$ (Walker, Ludford & Hunt[8], equation (5)). Now the core flow can be analysed using equations (2.2) and the boundary conditions (2.4) and (2.6).

These conditions can be applied to Kulikovskii's general solution to obtain solutions for non-conducting ducts. However, it is more instructive to obtain

these results by heuristic physical arguments. Consider flow along the non-conducting duct shown in Fig.3 where both the cross-section and $\underline{B}$ vary in the streamwise (z) direction. Equation (2.6) tells us that the component of the core current density normal to the wall is $O(M^{-1})$ which implies that so far as the $O(1)$ core variables Φ' and $\underline{v}'$ are concerned, $\underline{j}' = 0$ in the core. Therefore, from equation (2.2c)

$$\nabla\Phi' = \underline{v}' \wedge \underline{B}' \tag{2.7}$$

It is interesting to note that even though we are analysing flows in which $R_m << 1$, equation (2.7) is satisfied by perfectly conducting fluids (i.e. $\sigma = \infty$) when $R_m = \infty$ (Shercliff[4], sec.3.4). From equation (2.7) it may be shown that the magnetic flux enclosed by an elemental fluid loop remains constant as it travels through the flow (see Appendix II). The difference between this flow and that where $R_m = \infty$ is that in the latter case the elemental fluid loop always encloses the same magnetic field lines whereas here it slips through them but in such a way that the flux linked is constant.

Consider now a slim tube of fluid, spanning the duct and moving with the flow such that at any instant the generators of its surface are coincident with field lines (see Fig.3). At any station along the duct it has a total length $S_o(x',z')$ (this being a function of its position) and its elemental cross-sectional area $\delta A'$ varies with s, the distance measured along the tube. Since the fluid is incompressible and effectively inviscid and since there is no flow through the walls (equation (2.4)) it follows that

$$\int_o^{S_o} \delta A'(s)ds = \text{constant} \tag{2.8}$$

It may be shown that if this tube is initially aligned along the field lines then it will continue to be so (see Appendix II). Since the flux linked is constant then

$$|\underline{B}'(s)|\delta A'(s) = \text{constant} \tag{2.9}$$

and so combining equations (2.8) and (2.9) leads to

$$\int_o^{S_o} \frac{ds}{B'} = I \tag{2.10}$$

where I is a constant for each fluid tube.

This result was derived formally from equations (2.2) by Kulikovskii[9] and independently, but from physical arguments similar to those used here, by Holroyd & Walker[10].

Equation (2.10) is the most important equation in this report; indeed it is of great significance in MHD duct flow literature. It implies that in the limit $N \to \infty$ the flow travels along what we will call 'characteristic surfaces', defined as those surfaces in the duct on which I = constant. These surfaces may turn back on themselves; they do not necessarily extend from far upstream to far downstream of some region where the shape of the duct and/or $\underline{B}'$ vary. In some cases the surfaces may have singular and indeterminate behaviour; an example is a variable

area rectangular duct in which the generators of the walls are parallel and perpendicular to the field lines of a uniform magnetic field as shown in Fig.4a. Such cases are discussed in more detail in secs.2.6 and 3.5.

In general, these 'characteristic surfaces' indicate the general feature of the flow. For example, in Figs.4b and 4c there is a speeding up of the flow near the sides of the pipe and a corresponding reduction in velocity near the centre of the duct. Indeed, in some cases a tube of stagnant fluid can form there parallel to the field lines. However, the actual velocity profiles and pressure variations across a region of non-uniformity can only be found by more detailed calculations. The reason is that the fully-developed flow upstream does not suddenly become transformed into flow along 'characteristic surfaces' in the region of non-uniformity. Inspection of the flows in Figs.4b and 4c shows that the electric potentials across these two ducts far upstream and downstream of their non-uniform regions, say $\Delta\Phi'_1$ at section z'_1 and $\Delta\Phi'_2$ at section z'_2, are different; in the former case because of the change in mean velocity and in the latter case because of the change in field strength. There is, therefore, a tendency for second order $O(M^{-\frac{1}{2}})$ electric currents to circulate in the streamwise direction. Order of magnitude arguments or detailed calculations show that these currents persist for large distances, of $O(\text{duct radius} \times M^{\frac{1}{2}})$, both upstream and downstream of the non-uniform region[10,11]. It is these recirculating currents which determine the pressure changes and the velocity distributions.

Detailed calculations for various ducts are given in sec.3 and some experimental confirmation is provided in sec.4.

2.4 Ducts with thin conducting walls ($M^{-1} \ll \phi \ll 1$)

At the surface of a duct with conducting walls the electrical boundary conditions are

continuity of component of $\underline{j}'$ normal to wall $$-\frac{\partial\Phi'}{\partial n'} = \underline{j}'.\hat{n} = -\frac{\sigma_w}{\sigma}\frac{\partial\Phi'_w}{\partial n'} \qquad (2.11)$$

continuity of component of $\underline{E}'$ tangential to wall $$\nabla\Phi' \wedge \hat{n} = \nabla\Phi'_w \wedge \hat{n} \qquad (2.12)$$

where Φ'_w is the electric potential in the wall. Equation (2.12) follows from equation (2.2c) since $\underline{v}' \equiv 0$ at the wall. Since equation (2.2d) is valid in the wall, then for a thin wall of thickness t ($\ll a$)

$$\underline{j}'.\hat{n} = -\left(\frac{\sigma_w}{\sigma}\right)\left(\frac{t}{a}\right)\nabla^2\Phi'_w = -\phi\nabla^2\Phi'_w \qquad (2.13)$$

where ∇^2 is the Laplacian operator in the surface of the duct (i.e. it does not contain the derivative $\partial^2/\partial n'^2$) (see Appendix I[1]). Since the electric field parallel to the wall only changes by $O(M^{-1})$ through a Hartmann boundary layer, it follows that if $\Phi' \gg M^{-1}$ then the boundary condition on the core flow is

$$\underline{j}'_\infty.\hat{n} = -\phi\nabla^2\Phi' \quad \text{as} \quad n' \to \infty \qquad (2.14)$$

Since we are assuming that $\phi \ll 1$, equation (2.14) implies that to first order

$$\underline{j}'_\infty.\hat{n} = 0 \qquad (2.15)$$

which is the same condition as on the current density in the case of a conconducting duct discussed in sec.2.2.

The boundary condition on the core velocity is also the same as that for a non-conducting duct, namely equation (2.4).

Therefore, to first order, $\underline{v}'$ and $\underline{j}'$ satisfy the same equations and boundary conditions in these two types of duct. Consequently, in a thin-walled duct the flow must also travel along 'characteristic surfaces' as defined by equation (2.10), but the velocity and pressure distributions are determined by the second order ($O(\phi^{\frac{1}{2}})$) currents recirculating in the streamwise direction which have to match the weaker $O(\phi)$ currents circulating in Oxy-planes in the fully-developed flows upstream and downstream. This is the reason for the large differences in the flows between thin-walled and non-conducting ducts when the shape of the duct and/or $\underline{B}'$ change (see sec.3.1).

2.5 Ducts with highly conducting walls ($\phi >> 1$)

If the walls of a duct are very highly conducting so that $\phi >> 1$, then equation (2.14) implies that the potential in the wall, Φ_w', satisfies

$$\nabla^2 \Phi_w' = 0 \tag{2.16}$$

Unless current is supplied to the wall from an external source, the only solution to equation (2.16) is

$$\Phi_w' = \text{constant} \tag{2.17}$$

Since $\Phi_w' = \Phi'$ and the potential change through a Hartmann boundary layer is only $O(M^{-1})$, then taking the value of the constant in equation (2.17) as zero it follows that if $\phi >> 1$

$$\Phi' = 0 \quad \text{at} \quad n' = 0$$

and so

$$\Phi_\infty' = 0 \quad \text{as} \quad n' \to \infty \tag{2.18}$$

Since the boundary condition on the core flow velocity, equation (2.4), still holds, it follows from equations (2.2c) and (2.18) that

$$\underline{j}' \wedge \hat{n} = (\underline{v}' \wedge \underline{B}') \wedge \hat{n} \quad \text{as} \quad n' \to \infty \tag{2.19}$$

No general form of Kulikovskii's solution (Appendix I) has been found for highly conducting walled ducts but some particular solutions have been found which will be described in sec.3.2. An important general conclusion concerning the electric potential distribution in the core from the solution (see equation (AI.3) in Appendix I) is that if $\underline{B}'$ is uniform then boundary condition (2.18) implies that $\Phi' \equiv 0$ throughout the flow. However, if $\underline{B}'$ is non-uniform such that $\underline{B}' \wedge \nabla B'^{-2} \neq 0$ then $\Phi' \neq 0$ in the core flow.

For a uniform magnetic field the general form of the solution may be derived from the equations in Appendix I or by inspection of equations (2.2). Letting $\underline{B}' = (0, B_y' = 1, 0)$ then $\Phi' = j_y' \equiv 0$ throughout the core and

$$v_x' = j_z' = -\frac{1}{N}\frac{\partial p'}{\partial x'} \qquad v_z' = -j_x' = -\frac{1}{N}\frac{\partial p'}{\partial z'}$$

$$v'_y = \frac{y'}{N}\left\{\frac{\partial^2 p'}{\partial x'^2} + \frac{\partial^2 p'}{\partial z'^2}\right\} + g(x',z')$$

The non-dimensional pressure $p'(x',z')$ and the unknown function of integration $g(x',z')$ are determined by satisfying equation (2.18) at the boundaries of the core flow at the upper and lower walls of the duct, say $Y_U(x',y',z') = 0$ for $y' > 0$ and $Y_L(x',y',z') = 0$ for $y' < 0$. The conditions are

$$-\frac{\partial p'}{\partial x'}\frac{\partial Y}{\partial x'} + \frac{\partial Y}{\partial y'}\left\{\left(\frac{\partial^2 p'}{\partial x'^2} + \frac{\partial^2 p'}{\partial z'^2}\right) + g\right\} - \frac{\partial p'}{\partial z'}\frac{\partial Y}{\partial z'} = 0$$

where Y may be either Y_U or Y_L. Eliminating $g(x',z')$ between these two equations leads to a second-order linear partial differential equation for $p'(x',z')$.

To avoid unphysical singularities in the pressure distribution $p'(x',z')$, conditions may have to be placed on the regularity of the derivatives of p' at certain points around the duct wall[12].

Detailed calculations of the flows in rectangular and circular ducts of variable cross-sectional area with highly conducting walls situated in transverse, uniform magnetic fields have been carried out by Walker & Ludford[12,13]. From their work, and ours in sec.3.4, it is possible to draw some general conclusions about flows in ducts with highly conducting walls situated in transverse magnetic fields, be they uniform or non-uniform.

(i) The fully-developed flow found in a straight pipe in a uniform transverse field is realised within a few duct radii upstream or downstream of a region where the cross-section of the duct and/or $\underline{B}$ varies.

(ii) The pressure gradient remains of $O(\sigma v_o B_o^2)$ even in non-uniform regions.

(iii) Changes in the velocity profile along the duct, $u^{-1}\partial u/\partial z$, are of the same order as the slope of the duct wall, $Y^{-1}\partial Y/\partial z$, or, we conjecture on the basis of sec.3.4, of the magnetic field gradients $B^{-1}\partial B/\partial z$.

2.6 Narrow layers parallel to the magnetic field lines

In the core flow analysis using equations (2.2) it is assumed that the inertial terms and viscous terms are negligible because $N \gg 1$ and $M \gg 1$ and because the velocity is assumed to vary over distances comparable with the radius of the duct. However, abrupt changes in either the slope or electrical conductivity of any boundary surface can lead to the development of large velocity gradients whose magnitudes are limited by the inertial and/or viscous terms which have been neglected in the first approximation. In other words, these discontinuities must, in fact, be extremely thin layers of finite thickness δ, the nature of which are determined by the relative magnitudes of M and R_e and by the nature and orientation with respect to both the magnetic field lines and the mean flow direction of the discontinuity.

If the magnetic field is large enough (a sufficient, but not always necessary,

condition being $M^{\frac{1}{2}} >> R_e$) or if there is no flow normal to the layer, then their thickness is determined by a balance between electromagnetic and viscous stresses. In that case equation (2.1a) reduces to

$$0 = -\nabla p' + N\underline{j}' \wedge \underline{B}' + \frac{1}{R_e} \frac{\partial^2 \underline{v}'}{\partial \zeta^2}$$

for a two-dimensional layer, the normal to which is designated by ζ . Taking $\underline{j}'$ and $\underline{v}'$ to be $O(1)$, then this equation suggests that

$$\delta/a \approx kM^{-\frac{1}{2}}$$

Typically the numerical factor is never found to be more than 5 .

In the proposed fusion reactor flows, however, $M^{\frac{1}{2}} << R_e$ and so the balance in the layers is between inertial and electromagnetic stresses (provided there is flow normal to the layer). Equation (2.1a) now reduces to

$$\underline{v}'.\nabla \underline{v}' = -\nabla p' + N\underline{j}' \wedge \underline{B}'$$

and inspection of it suggests that

$$\delta/a \approx kN^{-1/3} \qquad (2.20)$$

where k has been found to be about 5 (Hunt & Ludford[7], equation (4.28); Hunt & Leibovich[14]). These inertial/electromagnetic layers have not been analysed for non-uniform magnetic fields but order of magnitude arguments suggest that estimate (2.20) is still valid.

When there is no flow through these layers they are usually referred to as shear layers. (For a comprehensive review of many types of these layers in uniform magnetic field situations see Hunt & Shercliff[15].)

In the MHD duct flows currently considered for fusion reactors the main causes of discontinuities in the flow are

(i) changes in the slope of the pipe walls (including bends)

(ii) junctions of two or more pipes

(iii) pipes ending, say, inside a reservoir into which they discharge fluid

(iv) changes in magnetic field strength and direction

The positions of the discontinuities, and hence the layers, are easily discerned in any design by simply noting where the 'characteristic surfaces' have discontinuities or suddenly change direction (see Fig.1b). Examples of such layers are denoted by 'S' in Figs.1a,b.

Since these layers are at least $M^{\frac{1}{2}}$ times thicker than Hartmann layers the boundary conditions on the flow in them where they meet walls at which there are Hartmann layers are the same as for the core. The other condition on them is that they must match the core flows on either side as $|\zeta| \to \infty$.

Generalising from those flows studied so far we find that

(i) if the walls of the duct are of uniform conductivity and have no significant portion parallel to the magnetic field lines, then a discontinuity in their slope with respect to the field lines produces layers but without any significant velocity or pressure gradient excesses

in the layer[11,12].

(ii) if some significant portion of the walls of the duct is parallel to the field lines and is either non-conducting or poorly conducting (i.e. $\phi << 1$) then changes in the field strength or cross-sectional area of the duct produce large velocity excesses in the boundary layers on those walls. These are one example of the class of layers where an $O(1)$ change of Φ' is found across the layer. They can also generate significant pressure gradients along the flow (see sec.3.3).

(iii) if from a pipe situated in a transverse magnetic field fluid is ejected into a larger volume of fluid or if the pipe bends through a right angle such that it becomes parallel to the field lines then, provided N is large enough, the flow runs parallel to the field in very thin layers of thickness $O(aM^{-\frac{1}{2}})$ or $O(aN^{-1/3})$ rather than across it. Along such layers there can be a significant pressure gradient and, obviously, the flow pattern is totally different from that in the absence of the field even though the flow may be in a pipe eventually parallel to the field.

3. EFFECTS OF NON-UNIFORM MAGNETIC FIELDS AND DUCT AREA CHANGES ON PRESSURE DROPS; THEORY

3.1 Circular non-conducting and thin-walled ducts

In this section we mainly consider flows in straight ducts placed in non-uniform magnetic fields but we draw attention to the similarities with flows in ducts whose cross-sectional area changes situated in uniform, transverse magnetic fields. Because they have much in common, we concentrate here on flows in ducts with non-conducting or thin conducting walls (i.e. walls for which $\phi << 1$). Some general properties of these flows have already been given in secs.2.3 and 2.4.

Consider a circular duct of radius a placed in a magnetic field $\underline{B}$ defined as

$$\begin{aligned} \underline{B} &= (0,B_o,0) && \text{for} \quad z < -\lambda a \\ \underline{B} &= (B_x,B_y,B_z) && \text{for} \quad -\lambda a < z < \lambda a \\ \underline{B} &= (0,(1-\alpha)B_o,0) && \text{for} \quad z > \lambda a \end{aligned} \tag{3.1}$$

where B_o is constant, λ satisfies $\lambda << M^{\frac{1}{2}}$ in a non-conducting duct and $\lambda << \phi^{-\frac{1}{2}}$ in a thin walled duct and $\alpha = O(1)$. The 'characteristic surfaces' in the duct for such a field are sketched in Fig.4c.

Clearly, the induced potential difference across the duct when $z << -\lambda a$ ($\approx 2v_oB_oa$) is greater than that when $z >> \lambda a$ ($\approx 2(1-\alpha)v_oB_oa$). Thus, there is a streamwise potential gradient which induces a streamwise current flow, j_z, which extends over the length ℓa of the duct. The following order of magnitude argument shows that $\ell >> \lambda$. From equation (2.2c)

$$j_z \approx \frac{\sigma v_o B_o a - \sigma(1-\alpha)v_o B_o a}{\ell a} \approx \frac{\alpha\sigma v_o B_o a}{\ell a}$$

and for continuity of current flow, equation (2.2d) implies that

$$j_x \approx aj_z/\ell a \approx \alpha\sigma v_o B_o/\ell^2 \qquad (3.2)$$

j_x, though, must be of the same order as the uniform transverse current flow in the fully developed flows that are realised far upstream and downstream where the duct is straight and the field strength uniform. Shercliff[16] shows that

$$j_x \approx \sigma v_o B_o M^{-1} \quad \text{in a non-conducting duct} \qquad (3.3a)$$

$$\approx \sigma v_o B_o \phi \quad \text{in a thin-walled duct} \qquad (3.3b)$$

Therefore equations (3.2) and (3.3) are only compatible if

$$\ell \approx M^{\frac{1}{2}} \quad \text{in a non-conducting duct} \qquad (3.4a)$$

$$\approx \phi^{-\frac{1}{2}} \quad \text{in a thin-walled duct} \qquad (3.4b)$$

(Mathematical support for these arguments may be found in Holroyd & Walker[10] and Walker & Ludford[11,17].) For the fusion reactor parameters quoted in sec.1.2, expressions (3.4) imply that the effects of even an extremely short length of non-uniform magnetic field in non-conducting and thin-walled ducts will be felt over distances of $O(100a)$ and $O(10a)$ respectively both upstream and downstream of the non-uniform field region.

Having estimated the strength of the recirculating currents induced by the non-uniform field, we can now establish more definite criteria for the neglect of inertial stresses than simply $N >> 1$. In the non-uniform field region ($-\lambda a < z < \lambda a$), equation (2.2d) shows that

$$j_x \approx aj_z/\lambda a \approx \alpha\sigma v_o B_o/\ell\lambda$$

Since α is $O(1)$ then the ratio of the electromagnetic and inertial stresses in this region is

$$\frac{|\underline{j} \wedge \underline{B}|}{|\rho \underline{v}.\nabla \underline{v}|} \approx \frac{j_z B_o}{\rho v_o^2/\lambda a} \approx \frac{N}{\ell}$$

Using the definitions of ℓ given by expressions (3.4), it follows that inertial stresses may be neglected if

$$NM^{-\frac{1}{2}} >> 1 \quad \text{i.e.} \quad M^{3/2} >> R \quad \text{in a non-conducting duct} \qquad (3.5a)$$

$$N\phi^{\frac{1}{2}} >> 1 \quad \text{in a thin-walled duct} \qquad (3.5b)$$

Both of these criteria are easily satisfied by fusion reactor parameters but are not so easily satisfied in laboratory experiments.

From a practical point of view the most important effect of non-uniform magnetic fields and changes in the cross-sectional area of the duct is that the pressure gradients are increased enormously. These gradients can be estimated by order of magnitude arguments and the estimates can in turn be supported by mathematical argument[10,11,17]. To appreciate their magnitudes it should be borne in mind that in a fully developed flow (i.e. straight duct and uniform, transverse magnetic field) the streamwise pressure gradient

$$dp/dz \approx \sigma v_o B_o^2/\ell^2 \qquad (3.6)$$

where ℓ is $M^{\frac{1}{2}}$ in a non-conducting duct and $\phi^{-\frac{1}{2}}$ in a thin-walled duct[16]. In

the regions where the fully-developed flow is disturbed by the recirculating current, i.e. $-\ell a < z < -\lambda a$ and $\lambda a < z < \ell a$, there is an additional pressure gradient, say $d\bar{p}/dz$, due to the component j_x of the circulating current. Since this j_x is of the same order as the fully developed flow j_x then $d\bar{p}/dz$ is of the same order as dp/dz in equation (3.6), but it takes opposite signs upstream and downstream of the non-uniform region because j_x moves in opposite directions. It follows, then, that an additional fall (or rise) in the pressure in the pipe over the length ℓa can occur, say $\Delta\bar{p}$, which from equations (3.4) and (3.6) may be estimated as

$$\Delta\bar{p} \approx \alpha\sigma v B_o^2 a M^{-\frac{1}{2}} \qquad \text{in a non-conducting pipe}$$

$$\approx \alpha\sigma v B_o^2 a \phi^{\frac{1}{2}} \qquad \text{in a thin-walled pipe}$$

Note that if the field rises in the streamwise direction, $\alpha < 0$ and so $\Delta\bar{p}$ is negative. Thus, for example, a large peak pressure will be found as a flow enters a region of magnetic field.

If such peak pressure rises can occur, then the pipe may have to be strengthened. However, the obvious method of doing this, namely by increasing the wall thickness of the pipe, is undesirable since it will increase ϕ and hence the pressure gradients and hence the total pressure loss.

The rise and fall in the pressure upstream and downstream of the non-uniform field region due to the recirculating current do not exactly cancel each other out. There is in fact a net pressure drop, $\Delta p < |\Delta\bar{p}|$, introduced into the pressure distribution. The pressure distributions along and the variation of the pressure drop Δp with α in circular non-conducting and thin-walled ducts are shown in Figs.5, 6, 7 and 8 respectively. Note how the abscissae in Figs.5 and 7 are compressed by scaling them on $M^{\frac{1}{2}}$ and $\phi^{-\frac{1}{2}}$ respectively. Thus, the non-uniform field region, $-\lambda a < z < \lambda a$, is compressed into a narrow region near $z = 0$. These figures show that for a flow moving to a weaker magnetic field the negative pressure gradient is increased upstream of the non-uniform field region where j_x is augmented by the recirculating current but just downstream of the non-uniform field region positive pressure gradients occur. The pressure also varies considerably across the pipe.

Theoretical velocity profiles, streamlines and streamlines of the recirculating current in a circular non-conducting duct are shown in Fig.9 assuming, as in Figs.5-8, that N is large enough to satisfy condition (3.5a). If $N \gg 1$ but is not large enough to satisfy $N \gg M^{\frac{1}{2}}$ then the flow will not follow exactly the 'characteristic surfaces' in the non-uniform field region. In the uniform field region order of magnitude arguments suggest that the fully-developed flow is still disturbed over distances of about $aM^{\frac{1}{2}}$ but the effects of the inertial forces will mean that the flow develops differently and, in turn, this affects the flow in the non-uniform field region as well.

For a thin-walled duct condition (3.5b) is easily satisfied either in a reactor duct or in laboratory experiments. However, in deducing that the flow travels along the 'characteristic surfaces' in thin-walled ducts we assumed that ϕ is so small that the ratio

$$\frac{\text{current entering wall}}{\text{recirculating current}} \approx \frac{\phi \nabla^2 \Phi'_w}{\phi^{\frac{1}{2}}} \approx \phi^{\frac{1}{2}} << 1 \qquad (3.7)$$

since $\nabla^2 \Phi'_w \approx O(1)$. This condition is hardly satisfied by the larger values of ϕ likely to be found in fusion reactor pipework and so the flow will resemble that in a highly conducting walled duct (discussed in sec.3.4) more closely than that in a non-conducting duct.

3.2 Bends in non-conducting and thin-walled ducts in a uniform magnetic field

For non-conducting or thin-walled pipes containing bends in a plane normal to $\underline{B}$ the 'characteristic surfaces' are not displaced relative to the pipe axis, they follow the pipe round. Thus, no large changes in the flow or in the pressure gradient are expected. However, the vorticity of the core flow parallel to $\underline{B}$ is changed by the bend by an amount of $O(a/R)$ where R is the radius of curvature of the bend. Consequently, when $N >> 1$ there will be a local change in the pressure gradient of $O(a/R)$ but no significant effects will be felt upstream or downstream of the bend.

For pipe bends in a plane parallel to the magnetic field lines the 'characteristic surfaces' are displaced towards the walls $|x| = a$ as shown in Fig.10 where the duct has turned through an angle of about 60^o. If the bend is increased to 90^o so that the pipe is aligned parallel to the field lines, the flow will be confined to narrow jets of thickness δ at the side of the duct. δ depends upon the relative magnitudes of M and R_e as discussed in sec.2.6. The thickness of these layers has not been determined for a circular duct but in a rectangular duct order of magnitude arguments based on the theory in sec.2.6 dictate that

$$\begin{aligned} \delta/a &\approx M^{-\frac{1}{2}} \quad \text{if} \quad M^{\frac{1}{2}} >> R_e \\ &\approx N^{-1/3} \quad \text{if} \quad M^{\frac{1}{2}} << R_e \end{aligned} \qquad (3.8)$$

In both cases the thickness increases as the flow moves downstream.

Since the fluid is confined to these jets which grow, albeit slowly, the wall shear stresses are large and there must be some current crossing the magnetic field. Both these effects produce much larger pressure gradients, $(dp/dy)_{//}$, along this part of the duct than are found in hydrodynamic flow, $(dp/dy)_v$, even though the magnetic field is parallel to the pipe axis. From equations (3.8) it follows that

$$\frac{(dp/dy)_{//}}{(dp/dy)_v} \approx M \quad \text{if} \quad M^{\frac{1}{2}} >> R_e \qquad (3.9a)$$

$$\approx N^{2/3} \quad \text{if} \quad M^{\frac{1}{2}} << R_e \,, \; N >> 1 \qquad (3.9b)$$

It is interesting to note that in the experiment carried out by Young, Holcomb & Fraas[18] at Oak Ridge where the pressure gradient was measured in a rectangular

duct parallel to the magnetic field just after it had turned through 90^{o} , it was observed that

$$(dp/dy)_{//} / (dp/dy)_{v} \approx 100$$

In their experiment, $M \approx 3000$, $R_e \approx 7000$ so that $N \approx 1200$. Thus $M^{\frac{1}{2}} << R_e$, $N >> 1$ and $N^{2/3} \approx 100$ in agreement with out estimate (3.9b).

Note also that upstream of a bend such as this the flow will be disturbed by currents circulating axially because the downstream induced electric field is zero (eventually) much like the flows along ducts whose area changed or the field strength changed. Thus, there will be an additional pressure drop $\Delta\bar{p}$ upstream of the bend where

$$\Delta p \approx \sigma a v_o B_o^2 M^{-\frac{1}{2}} \qquad \text{in a non-conducting duct}$$
$$\approx \sigma a v_o B_o^2 \phi^{\frac{1}{2}} \qquad \text{in a thin-walled duct}$$

3.3 Junctions of pipes

Where junctions between non-conducting and thin-walled pipes occur the analysis used for bends can be applied with little modification. The first step is to trace out the 'characteristic surfaces' and the second is to consider the development of the flow upstream and downstream of the bends that are thus located. Sudden changes in the direction or abrupt termination of the 'characteristic surfaces' point to the existence of shear layers in the flow (see sec.2.6 and Fig.1b).

These ideas cannot be applied to junctions of highly conducting pipes. However, our discussions of flows in such ducts in secs.2.5 and 4.5 suggest that any disturbance of the meeting flows will be confined to the immediate vicinity of the junction.

3.4 Circular highly conducting walled ducts

No general or particular solution has been found for the flow in ducts with highly conducting walls in a non-uniform field. However, Holroyd[19] developed a solution for cases where there are only slight changes in $\underline{B}'$. Thus, in the magnetic field defined by equations (3.1), $\alpha << 1$. In such a case $\underline{B}'$ and the core flow variables can be expanded as power series:

$$\underline{B}' = \underline{B}^{(0)} + \alpha\underline{B}^{(1)} + \alpha^2\underline{B}^{(2)} + \ldots \qquad \underline{v}' = \underline{v}^{(0)} + \alpha\underline{v}^{(1)} + \alpha^2\underline{v}^{(2)} + \ldots$$

where the zero order solution ($\underline{B}^{(0)}, \underline{v}^{(0)}$ etc.) corresponds to the fully developed flow upstream. Substituting these series into equations (2.2) and making use of boundary condition (2.18) leads to an inhomogeneous partial differential equation for the first order pressure term $p^{(1)}$. Holroyd then found an approximate power series solution for $p^{(1)}$ in a circular duct, and thence derived expressions for $\underline{v}^{(1)}$ etc.

This theory shows that the disturbance to the flow is now confined to the non-uniform field region and that the pressure gradient remains of the same order as its fully developed flow value, namely

$$dp/dz \approx \sigma v_o B_o^2$$

The fractional change in the mean velocity in the non-uniform field region is $O(\alpha)$ in line with our generalisation in sec.2.4.

Later, in sec.4.5, pressure distributions and velocity variations measured in a highly conducting walled duct will be compared with corresponding theoretical distributions derived from the above theory.

Since the currents in the duct are $O(\sigma v_o B_o)$, it follows that a sufficient condition for inertial stresses to be neglected is $N \gg 1$. This is a weaker condition than those for non-conducting and thin-walled ducts analysed in sec.3.1.

3.5 Rectangular ducts with constant wall conductivity

The analysis of secs.2.2 and 2.4 and the methods of secs.3.1 and 3.2 are applicable for a wide range of shapes of duct and non-uniform magnetic fields. However, it is possible to envisage cases in which the 'characteristic surfaces' are indeterminate making the previous analysis irrelevant. Fig.4a shows an example of such a degenerate case being a non-conducting rectangular duct with its side walls parallel to a uniform magnetic field and its top and bottom walls diverging. If the cross-section of this duct is taken as the limit of a deformed elliptical duct then the effect of the area change is to make the 'characteristic surfaces' move abruptly to the side walls. In Fig.4a, the flow is diverted from the core upstream to the walls in a narrow layer spanning the duct of thickness either $O(aM^{-\frac{1}{2}})$ or $O(aN^{-1/3})$ (see sec.2.6). Analogous examples with non-uniform magnetic fields are not hard to find but the detailed form of the field must be known to determine whether or not the previous analysis still applies.

Using this last argument for a duct with non-conducting walls leads us to conclude that the bulk of the flow is confined to boundary layers of thickness δ adjacent to the side walls parallel to the field lines, while the core velocity is only $O(v_o \delta/a)$. Thus the velocity in these side wall boundary layers is $O(av_o/\delta)$. These qualitative arguments are supported by asymptotic analysis based on equations (2.2) as $N \to \infty$ [8]. As was shown in sec.2.6, if

$$M^{\frac{1}{2}} \gg R_e \quad , \quad \delta/a \approx O(M^{-\frac{1}{2}}) \tag{3.10a}$$

but if

$$N \gg 1 \quad \text{and} \quad M^{\frac{1}{2}} \ll R_e \quad , \quad \delta/a \approx O(N^{-1/3}) \tag{3.10b}$$

In either limit, the second being more relevant to fusion reactor calculations, the boundary layers are very thin.

The only experiments that have been performed using such ducts have been for values of $N < 1$. Even so, the predicted high velocities in the side wall boundary layers have been observed (Branover & Shcherbinin[20]; Slyusarev, Shilova & Shcherbinin[21]).

As with other ducts, the effect of an increase or decrease in magnetic field strength is to provide a path for a streamwise electric current circulation (see Walker, Ludford & Hunt[8], Fig.3). This leads to an increase in the pressure gradient. In the limit (3.10a) for a variable area duct, the fully developed flow

pressure gradient of $O(\sigma v_o B_o^2 M^{-1})$ is increased by a factor of $M^{\frac{1}{2}}$ to $O(\sigma v_o B_o^2 M^{-\frac{1}{2}})$, and remains of the same order across the whole cross-section (unlike that in a circular duct). Note also that the fully developed flow is only disturbed over a few duct widths immediately upstream and downstream of the expansion. It seems reasonable to expect that a non-uniform magnetic field would produce similar effects.

In a variable area rectangular duct with highly conducting walls, Walker & Ludford[13] show that the pressure gradient remains of $O(\sigma v_o B_o^2)$, and it is to be expected that it remains so in a non-uniform magnetic field.

3.6 Rectangular ducts with mixed wall conductivities

A type of rectangular duct found in many MHD laboratory experiments (but unlikely to be found in fusion reactor pipework) has a pair of highly conducting walls parallel to each other and the field lines, and the other walls non-conducting (see Fig.11). Should the field be non-uniform then it must vary only in planes parallel to the conducting walls (i.e. there is no variation across the duct). In such ducts, should the field strength decrease along the duct or should the non-conducting walls diverge then currents will flow along the conducting walls from regions of high to low induced electric field, $\underline{v} \wedge \underline{B}$, as indicated in Fig.11. This points to a non-uniform pressure gradient along the duct.

It is instructive to analyse this particular duct flow a priori rather than by means of Kulikovskii's general solution. The advantage of studying this particular type of duct flow is that the analysis is valid for the range of N and variation of $\underline{B}$ found in our experiments. If the conducting walls are assumed to be perfectly conducting then the electric field component E'_x is constant along the duct, say E_o (which implies that $E'_y = E'_z \equiv 0$), j_z (in the fluid), j_y and v_x are all negligible and the remaining non-zero core variables are independent of the x co-ordinate. It therefore follows from equations (2.2a) and (2.2c) that

$$(\underline{B}'.\nabla)j'_x = 0 \quad \text{so that} \quad \underline{j}' = (j'_x(A),0,0)$$

where $A(y',z')$ is constant along a magnetic field line (it is, in fact, part of the magnetic vector potential $\underline{A}$ defined in equation (2.2g)). By deriving the velocity components from a stream function $\Theta(y',z')$ so that $\underline{v} = -\nabla \wedge (\Theta,0,0)$ equation (2.2b) is automatically satisfied and the only non-zero component of equation (2.2c) may be written as

$$j'_x = E_o + B' \frac{\partial \Theta}{\partial s} \tag{3.11}$$

where $\partial\Theta/\partial s$ is the velocity component in the $Oy'z'$ plane normal to a field line and s is the distance measured along that field line. From equation (3.11) it may be deduced that

$$\Theta = (j'_x - E_o) \int_o^s \frac{ds}{B'}$$

the integration being carried out along magnetic field lines. This solution automatically satisfies boundary condition (2.4) at the non-conducting walls. An

expression for the flow rate, along the duct, Q, can easily be derived from this expression and this can be related to the pressure gradient $dp/dz = j_x B_y$ as

$$\frac{dp}{dz} = B_y\left[E_o + \frac{Q}{4}\left(\frac{a}{b}\right)\left\{\int_o^{S_o} \frac{ds}{B}\right\}^{-1}\right]$$

where S_o is the total length of the field line between the non-conducting walls and $2b$ is the distance between the conducting walls. To complete the solution the value of E_o is required. This can be determined by integrating equation (3.9) over the area of the conducting walls, A_o', and equating the term

$$\iint_{A_o'} j_x' \, dy'dz'$$

to the total current, if any, supplied to the walls from any external source.

In practical cases the finite conductivity of the walls invalidates these results because the current flow along the walls leads to a longitudinal potential gradient i.e. E_o varies with z. For a straight duct in a non-uniform field a good approximation for the variation of E_o along it can be found by neglecting j_z in the fluid, j_y and v_y, and applying the thin-walled boundary condition at the conducting walls (even though they are not necessarily thin). Then it may be shown that $E_o(z)$ satisfies

$$\frac{d^2E_o}{dz^2} - m^2E_o = \tfrac{1}{2}m^2 v_o B_y'(z)$$

where $B_y'(z)$ is an average value of B_y' across the duct and $m^2 = 1/\phi b$. Use of the two relevant boundary conditions, namely that $j_z = 0$ at each end of the conducting walls, determines E_o. j_x' may then be calculated from the x-component of equation (2.1b) and thence p' from the z-component of equation (2.2a)[19].

A more detailed analysis of the problem by Holroyd[22], taking into account the longitudinal current flow in the fluid and the finite thickness of the conducting walls, but neglecting v_x, justifies the assumptions made in the above analysis.

4. LIQUID METAL MHD DUCT FLOW EXPERIMENTS AT CAMBRIDGE

4.1 Aims of the experiments

The aim of the experimental programme at Cambridge has been to test the theory of MHD duct flows when the magnetic field is effectively very large so that $N \gg 1$. Our main interest has been in measuring pressure, velocity and electric potential distributions in straight ducts situated in non-uniform, transverse magnetic fields. The application of the experimental results has been to aid the design of fusion reactor coolant flow circuits, but, of course, it is not possible in laboratory experiments, where mercury rather than lithium must be used, to obtain values of M, N and R_e comparable with those expected in reactor pipework such as are quoted in sec.1.2.

However, if the theory can at least be relied upon for correct scaling of the flow as M, N, R_e and ϕ vary, then laboratory measurements should be of some value

in designing a prototype. The scaling could be tested by taking measurements at various values of the parameters in the experiments. We designed our experiments to achieve values of $M < 600$, $N < 150$, $R_e < 9000$ and $\phi \approx 0$, 0.1 or 10. Such a parameter range can be realised with velocities and pressures just large enough for measurement. Higher values of N could only be obtained by decreasing the velocities but then in some cases satisfactory measurements become impossible.

4.2 Apparatus

A new MHD liquid metal flow circuit shown in Fig.12 had to be built for these experiments. Basically it is similar to previous circuits used by Alty[23] at Cambridge and Hunt[24] at the University of Warwick.

The magnetic field is provided by an iron-core C-magnet designed and manufactured at Culham Laboratory. Variations in the field strength along the air gap of the magnet could be produced by attaching suitably shaped pole pieces to the ends of the yoke. On the basis of computations at Culham, appropriate pole pieces were designed to produce a field that decreased by 50% from one uniform value to a lower uniform value - the step change field, Fig.13a, and a field in which a length of uniform field was followed by a length of steadily decreasing field strength - the slow change field, Fig.13b. In the slow change field there is a 40% decrease in the field strength over a length of about 10 air gap widths. From Figs.13a and b it can be seen that the maximum field strength, about 0.6 T, is obtained over a length of about 450 mm and an area of about 100×100 mm^2. These two fields allow the effects of both decrease in field strength and rate of decrease of field strength on the flow to be studied.

Mercury is used as the liquid metal because of its relative safety and ease of handling at room temperature, as well as allowing inexpensive flexible PVC tubing to be used. It is pumped from the lower weir tank by a stainless-steel gear pump (loaned to us by Dept. of Engineering, Univ. of Warwick) to a similar upper weir tank; between them they maintain a constant pressure head across the circuit and, hence a constant flow rate through it. Except for the overflow mercury which is returned directly to the lower weir tank, the main mercury flow is through a laboratory made electromagnetic flowmeter (similar to that used by Alty[23]) with a response of 20.5 cm^3/s per mV and then through the test duct to the lower weir tank. Flow rates up to 150 cm^3/s could be achieved.

Pressure differences are measured by an air-over-meths-over-mercury manometer built to a design used by Shercliff[16] which gives consistent readings down to about 0.1 mm meths.

The (steady) electric potential distribution within the flow is measured by a probe similar to that used by Hunt and Malcolm[25]. In non-conducting ducts velocities can be deduced from potential measurements using equation (2.7). Confirmation of these deduced velocities by direct measurement, as well as velocity

measurements in other ducts, are made with DISA hot film anemometry equipment using their hot film probes, specially designed for use in electrically conducting liquids. (Such probes comprise a 70 μm diameter quartz rod upon which is deposited an extremely thin layer of nickel which in turn is covered by a 2 μm thick layer of quartz to insulate the nickel from the fluid.) Reliable velocities of down to 2.5 mm/s were successfully measured with these probes which is significantly lower than the lower limit of 30 mm/s quoted by Malcolm[26].

Calibration of the probes was done in the highly-conducting walled circular duct (described below) where the velocity over the whole cross-section could reliably be assumed uniform when the magnetic field was uniform. For velocity measurements in this duct, it was first of all positioned so that the probe was in the highest uniform field region about midway between the end of the magnet and the position where the field strength changed along its length. In this position the velocity would be uniform and so the probe could be calibrated. The duct, complete with probe, was then moved until the probe was in the non-uniform field region and the required velocity measurements were made. For velocity measurements in the non-conducting duct the probe had to be transferred to it from the highly conducting duct after calibration.

Four different ducts were used in the experiments, each having 14 or 15 pressure tappings along its length. All were about 1.6 times as long as the magnet so that when moved relative to it the flow pattern, which is determined by the magnetic field, would not be affected. Apart from the second duct described below, all were fitted with probe traversing gear to enable hot-film and potential probes to be inserted into the flow to measure the velocity and electric potential distributions. Basic details of the ducts are as follows:-

(i) circular non-conducting walled duct - made from 78.2 mm ID x 5.53 mm wall ABS (plastic) tube

(ii) circular thin-walled conducting duct - in conjunction with Culham two ducts were designed for use with mercury with conducting walls such that both ϕ ($= \sigma_w t/\sigma a$) $<< 1$ and the contact resistance between the walls and the mercury was zero (thus simulating the expected lack of contact resistance between liquid lithium and niobium or stainless steel pipes in a fusion reactor). The only suitable material is copper for which $\sigma_w/\sigma \approx 60$ which requires $t/a \lesssim 0.002$ to satisfy $\phi \lesssim 0.1$.

In one design a length of the aforementioned ABS tube was divided longitudinally into two halves. Each half was lined internally with 0.125 mm copper shim and they were then clamped together. This assembly could only be used for pressure measurements since then the longitudinal plane of the breaks in the copper wall could be aligned with the plane of symmetry of the magnetic field, namely the mid-plane of the

air gap parallel to the pole faces, which is also the plane of symmetry of the internal current flow (i.e. there is no current flow across this plane and hence the breaks in the wall are unimportant).

In the second design a circular, slightly tapered ($\approx 0.05^{o}$) mandrel was electroplated (externally) with copper. After lapping with fibre-glass the mandrel can be knocked out leaving an internally plated tube with no breaks in the wall. Such a tube can be rotated about its axis allowing probes to be positioned almost anywhere over its cross-section.

With this plating thickness $\phi \approx 0.2$ and on the basis of the experimental results it remained so throughout the experimental programme thus belying the fears of Glaberson et al.[27] that mercury would quickly erode copper walls. Comparison of the measured pressure gradient in these ducts in a uniform magnetic field with the theoretical value derived from the theory of Chang & Lundgren[28] suggests that contact resistance became negligible once a proper amalgam had formed at the mercury/copper interface.

(iii) circular highly conducting walled duct - made from 82.5 mm ID x 6.35mm wall high conductivity copper pipe giving $\phi \approx 8.75$.

(iv) rectangular duct - the highly conducting side walls of high conductivity copper 6.35 and 9.5 mm thick were clamped to PVC non-conducting top and bottom walls by 42 stainless steel bolts passing through the latter. By appropriate use of washers, bushes and gaskets the duct was sealed and the conducting walls were electrically isolated from each other. Internal dimensions - 69.5 mm between non-conducting walls x 87.3 mms.

4.3 Measurements in the non-conducting duct

The pressure distribution along the duct for the step change field shown in Fig.13a is plotted in Fig.14 in the dimensionless form derived from the theory in sec.3.1. On account of the small pressure gradients in a non-conducting duct, all six sets of readings were taken at the highest obtainable magnetic field strengths and so in this case there could be no verification of the theoretical scaling laws for $\Delta\bar{p}$. In the highest uniform field region, the pressure, p, agrees quantitatively with the theory but in the non-uniform region the variation of p has only the same form as the theory near $z = 0$. The negative peak pressure is about twice as great as that predicted by the theory, and does not extend as far downstream as the theory suggests. Note also the positive peak pressure, $\Delta\bar{p} \approx 2\sigma a v_o B_o^2 M^{-\frac{1}{2}}$ where the flow enters the magnetic field.

Experiments were also carried out with the slow change field shown in Fig.13b. Then near $z = 0$ a negative peak pressure of about $0.4\sigma a v_o B_o^2 M^{-\frac{1}{2}}$ was recorded.

Velocity profiles in the flow with the step change field are shown in Fig.15 and it can be seen how in the non-uniform field region the fluid moves away from the

centre of the duct to the walls giving rise to what some authors describe as an M-shaped velocity profile. It is most probable that the M-shaped profile at $z/a = -5.18$ was created as the flow entered the magnetic field. The growth and decay of such profiles has been discussed by Shercliff[4] (sec.4.14), Branover[29] and Bocheninski et al.[30]. Upstream of the non-uniform field region the velocity of the flow at the centre of the duct increases from its fully developed value but in the non-uniform region the flow tends to follow the 'characteristic surfaces' (similar to those shown in Fig.4c) and the M-shaped velocity profile develops. Downstream of the non-uniform field region this profile slowly degenerates but the fully-developed profile is not realised because of the relatively short length of uniform field.

Discrepancies between theory and experiment stem from the fact that in the experiments

$$NM^{-\frac{1}{2}} \approx 30 \times (525)^{-\frac{1}{2}} \approx 1$$

and so condition (3.5a) is not satisfied. Since inertial effects cannot be neglected we can estimate an additional contribution to the negative pressure peak near $z = 0$ and it turns out to be about $-0.5\sigma a v_o B_o^2 M^{-\frac{1}{2}}$ for these experiments. Therefore, the excess pressure peak is explicable.

4.4 Measurements in the thin-walled duct

Since the mandrel-plated duct only became available towards the end of the experimental programme, experiments were restricted to pressure measurements. With $\phi \approx 0.2$ the pressure gradients were about 100 times larger than in the non-conducting duct (see equation (3.6)) and so reliable pressure measurements could be made over a range of field strengths; in particular N varied between 13 and 50 . The results for the step change field are plotted in Fig.16. In the uniform field regions the gradients are constant and in agreement with the theoretical values derived from the theory of Chang & Lundgren[28] which implies that the flow is fully developed (and, as we mentioned in sec.4.2, that contact resistance at the mercury/copper interface is, in fact, zero).

An important consequence of these results is that since the theory has been shown to be in agreement with measurements of liquid lithium flowing in stainless steel tubes (Carlson[31]) then mercury flowing in tubes with thin copper walls must be a good way of simulating liquid lithium flow in fusion reactor pipework.

In the non-uniform field region there is a large difference between the theoretical predictions described in sec.3.1 and the experimental results. The results show that the pressure can be plotted as $p/\sigma a v_o B_o^2 \phi^{\frac{1}{2}}$ against $z\phi^{\frac{1}{2}}/a$ but that the predicted negative peak pressure of about $0.24\sigma a v_o B_o^2 \phi^{\frac{1}{2}}$ is absent. In addition, the theoretical pressure drop $\Delta\bar{p} = 0.163\sigma a v_o B_o^2 \phi^{\frac{1}{2}}$ whereas in the experiments $\Delta\bar{p} = 0.4\sigma a v_o B_o^2 \phi^{\frac{1}{2}}$. However, both theory and experiment show that the adjustment length for the pressure is about $0.6a\phi^{-\frac{1}{2}}$. The reason for these

discrepancies is that in our experiments $\phi^{\frac{1}{2}} \simeq 0.44$ which hardly satisfies the theoretical condition (3.7) that $\phi^{\frac{1}{2}} << 1$. In other words, the longitudinal recirculating current is short-circuited through the conducting walls.

4.5 Measurements in the highly conducting walled duct

Even larger pressure gradients are produced in this duct and pressure differences could be measured to an accuracy of less than 1% over the range of N , 9.5-119 , employed. The results for the step change field are plotted in Fig.17 and in the uniform field regions the pressure gradients are in agreement with those derived from the theory of Chang & Lundgren[28] for a circular duct with a large but finite conductance ratio (ϕ = 8.75).

In the non-uniform field region the pressure distribution has the same form, qualitatively, as the theory, namely a steady reduction of the pressure gradient without any pressure peaks. However, the theoretical pressure drop $\Delta\bar{p} = 0.47\sigma a v_o B_o^2$ is greater than the experimental value of $0.25\sigma a v_o B_o^2$. A possible explanation is that since the theory is based on the assumption that $\alpha << 1$, the value of α used in the calculations (0.375) is too great for the theory to be accurate. (This value of α was chosen so as to give the correct pressure gradient in the lower field strength region of the step change field.)

The pressure variation with N is as predicted and so these results can confidently be extrapolated to higher values of N .

Fig.18 shows the velocity variation in the non-uniform field region. Results and theory are in agreement to within 2% which suggests that the theory is reasonably satisfactory and that the hot-film anemometry is reasonably reliable.

Equally good comparison between theory and experiment was found with the slow-change field. In that case the pressure gradient changes gradually and the velocity perturbations are smaller.

4.6 Measurements in the rectangular duct

Pressure measurements made in the rectangular duct described in sec.4.2 with the step change field are shown in Fig.19. They confirm the surprising theoretical prediction that the pressure rises in the region of lower field strength ($z > 0$). The reason is that this region acts as a return path for much of the current generated in the higher field strength region ($z < 0$). Since the theory is approximate and based on the assumption that $N >> 1$, it is not surprising that there is some discrepancy between theory and experiment for the pressure distribution where the flow enters and leaves the magnetic field since in these regions $N \to 0$.

Further confirmation of the theory comes from the measurement of the potential difference between the conducting walls of the duct along its length shown in Fig.20. Note how this varies as the position of the duct is changed relative to the magnetic field thus changing the current distribution in the walls and flow. In

addition these distributions are little affected by changes in N.

5. PRESSURE DROP REDUCTION AND FLOW IN BLANKET CELLS

5.1 Pressure drop reduction by change of duct cross-section

In Appendix I of Hunt & Hancox[1] it was pointed out that in thin walled ducts the pressure gradient required to drive a given flow rate along a duct of given cross-sectional area situated in a uniform, transverse magnetic field varied with the shape of the cross-section. For values of ϕ found in fusion reactor pipework this required pressure gradient should decrease as the duct is elongated in the direction of the field, e.g. the thin diamond shaped and slim rectangular ducts shown in Figs.21a and b respectively.

Using the analytical methods of Chang & Lundgren[28] it can be shown that provided $\theta >> M^{-\frac{1}{2}}$ in the diamond shaped duct

$$\frac{dp}{dz} = - \frac{Q\eta}{4a^4} M^2 \cot\theta \frac{\phi \sin\theta + M^{-1}}{\frac{1}{2}\phi \sin\theta + \frac{1}{3}} \qquad (5.1)$$

where Q is the volumetric flow rate and θ is the angle indicated in Fig.21a.

For the slim rectangular duct analysis by Temperley & Todd[32] indicates that velocities in the boundary layers of thickness $O(aM^{-\frac{1}{2}})$ on the walls parallel to the magnetic field will be larger by a factor of $O(M^{\frac{1}{2}})$ than those in the core (see Fig.21c) provided that the conductance along the walls is much larger than along the adjacent boundary layer, i.e. $\phi M^{\frac{1}{2}} >> 1$ for the side walls and $\phi M >> 1$ for the top and bottom walls. In such cases

$$\frac{dp}{dz} = - \frac{Q\eta}{4a^4} M^2 \frac{a}{b} \{1 + \frac{1}{\phi}(1 + \frac{a}{3b}) - \frac{0.3737}{\phi^2 M^{\frac{1}{2}}} \frac{b}{a} + O(M^{-1})\}^{-1} \qquad (5.2)$$

The following table shows how these pressure gradients compare with that in a circular duct for large values of M when the flow rate, field strength, cross-sectional area, wall thickness and conductivity are all equal. The values of ϕ quoted are for the circular duct.

ϕ	circular	diamond	rectangular
0.01	1	0.322	0.210
0.1	1	0.341	0.224
0.2	1	0.361	0.240

Experiments have been carried out using mercury in the ducts built to dimensions specified in Figs.21a and b. They were made by lining a PVC duct with 0.125 mm copper shim as described in sec.4.2 (subsection on circular thin-walled conducting duct) giving $\phi = 0.19$. In general, the pressure gradients measured in these ducts with a uniform magnetic field were less than those predicted by equations (5.1) and (5.2) by 6% and 18% respectively. In the latter case this discrepancy may be due to the fact that the theory, which assumes that a core flow exists, is not strictly applicable to such a slim duct because the boundary layers on its side walls are thick enough to meet at the centre. Nevertheless, the results point to the

existence of the predicted high velocities in these boundary layers.

In both ducts the pressure gradients decrease, possibly to an asymptotic value, as N increases but since $N \lesssim 55$ in the experiments this could not be proved conclusively. This dependence on N is interesting because in these experiments the flow should be fully developed in which case inertial effects ought to be absent. In the slim rectangular duct the results indicate that the pressure gradient near the inlet end is, on average, about 3% greater than at the outlet end but there is no systematic variation of this difference with N or M. However, it does suggest that the flow may not be truly fully-developed along part of the duct, possibly due to the disturbed flow near the inlet. The results for the diamond shaped duct do not exhibit the same features as those in the slim rectangular duct but that does not rule out the possibility that the flow may not be fully-developed. So far, no straightforward relationship between the pressure gradients, M and N, has been found.

5.2 Pressure gradient reduction in a circular pipe

The pressure drop along a circular thin walled pipe might be reduced by sub-dividing its cross-section into, for example, a number of diamond shaped cells, as shown in Fig.22a. In practice, a matrix of such cells could be inserted into straight lengths of pipe. The matrix need not be of robust construction because each of its walls is subjected to equal and opposite pressure loads on each side. However, to achieve a reduced pressure gradient, the electrical conductance between adjacent walls of neighbouring cells must be much less than $\sigma\phi$ so that electric currents cannot flow between neighbouring cells. Ideally all the cells should be electrically isolated from each other but this would be difficult to realise in practice.

In this ideal case Fig.22b shows how the flow rate increases for a fixed pressure gradient with the number of diamond cells of the matrix (Fig.22a shows a matrix with five diamond cells). The conductance ratios of the circular pipe and matrix walls are ϕ and ϕ/k respectively and are based on the radius of the former. It is assumed that M is large and reductions of the cross-sectional area due to the finite thickness of the matrix walls are neglected.

5.3 Coolant flow in blanket cells

Two possible methods for controlling the liquid lithium coolant flow when at its nearest to the plasma are shown in Figs.23a and 24a. Both aim to provide maximum 'wetting' of the surface receiving maximum radiation from the plasma.

At the top end of the cell shown in Fig.23a (see Stanbridge et al.[33] and Carruthers[34]), the coolant entering along the central pipe should ideally impinge on the surface directly ahead and follow it for some distance. However, in sec.2.6 we pointed out that a shear layer of maximum thickness $O(aN^{-1/3})$ will form parallel to the field lines where a flow emerges from a pipe into a reservoir of fluid.

Consequently the flow in this cell will be as sketched in Fig.23b. In addition there will be a current flow along this inlet pipe; if it is assumed that it is thin-walled but electrically isolated from the surrounding flow in the main body of the cell then these currents will be $O(\phi^{\frac{1}{2}}\sigma v_o B_o)$ (sec.2.3) and in the shear layer the current density will therefore be $O(N^{1/3}\phi^{\frac{1}{2}}\sigma v_o B_o)$. If part of this current flow is perpendicular to the field lines then the presence of the shear layer will add a large pressure drop to the pressure distribution in the cell of $O(N^{1/3}\phi^{\frac{1}{2}}\sigma v_o B_o^2) \approx O(N^{1/3}\phi^{\frac{1}{2}}$ a x fully-developed flow pressure gradient).

The formation of the shear layer will leave a volume of stagnant fluid trapped in the dome of the cell as shown in Fig.23b. This might vapourise thus affecting the heat transfer there.

A design for the inlet pipe which offers several advantages comprises two coaxial metal tubes of slightly different radii welded together at one end, possibly held apart by spiders in the annular gap between them, with the outer one attached to the main body of the cell at its point of penetration. With this construction there would be a very high electrical resistance connection between the inner and outer walls of the pipe, except near the welded end, which is highly desirable from a MHD point of view since the incoming and outgoing flows are then electrically isolated from each other, and thermal stresses are mitigated[33]. Exactly how this design would affect the detailed pressure and velocity distributions within the cell must remain a matter for conjecture at present.

As a first step towards increasing our knowledge about the flow in the cell, we have investigated the flow in a symmetric, circular, thin-walled annular duct. The analytical methods of Chang & Lundgren[28] may be used to show that the flow rate, Q , when such a duct is situated in a uniform, transverse magnetic field is related to the pressure gradient, dp/dz , by

$$\frac{Q\eta}{4a^4} = -\frac{1}{M}\frac{dp}{dz}\left[\frac{1+\phi}{\kappa}\left\{\frac{\frac{\pi}{2} - \sin^{-1}r - r(1-r^2)^{\frac{1}{2}}}{2} - \frac{1-r}{\kappa} + \frac{\frac{\pi}{2} - \sin^{-1}r}{\kappa^2} - \frac{1}{\kappa^2(\kappa^2-1)^{\frac{1}{2}}}\log\left(\frac{\varepsilon+1}{\varepsilon-1}\cdot\frac{\varepsilon-\xi}{\varepsilon+\xi}\right)\right\} + \int_o^r \frac{(f_1+f_2)f_1}{2+Mf_2}\,dx\right] \qquad (5.3)$$

where $f_1 = (1-x^2)^{\frac{1}{2}} + (r^2-x^2)^{\frac{1}{2}}$, $f_2 = \phi(1-x^2)^{\frac{1}{2}} + \phi_r(r^2-x^2)^{\frac{1}{2}}$, $\kappa = M\phi$, $\varepsilon = \{(\kappa+1)/(\kappa-1)\}^{\frac{1}{2}}$, $\xi = \tan(\frac{1}{2}\sin^{-1}r)$ and ϕ and ϕ_r are the conductance ratios of the tube and rod based on their respective radii.

Experiments have been carried out using mercury in such a duct comprising a 28.8 mm diameter perspex rod electroplated with a 0.06 mm thick layer of copper ($\phi_r = 0.24$) mounted co-axially inside a 74 mm diameter tube with a 0.09 mm thick copper wall ($\phi = 0.138$) (made by the mandrel plating technique described in sec.4.2 (subsection on thin conducting walled duct)). Pressure gradients measured

in this duct are up to 13% lower than predicted by equation (5.3) and for constant values of M the gradients decrease as N increases as happened in the experiments with the diamond shaped and slim rectangular ducts described in sec.5.1. In this case the results show that the pressure gradient near the ends of the rod is greater than that over its central section and this could be due to disturbances to the flow created by the spiders supporting the rod inside the tube of nearly twice its length.

In future experiments the rod will be replaced with a fibre-glass tube electro-plated with a thin layer of copper internally, externally and at one end thus simulating the welded connection in the actual cell entry pipe. Apart from measuring pressure distributions in this 'cell', it is hoped to investigate the behaviour of the flow as it leaves the entry pipe by using hot-film anemometry.

The second method of guiding the flow (shown in Fig.24a) has been proposed by research workers at Wisconsin (Badger et al.[36], Vol.1, sec.IV). A series of baffles, ideally aligned parallel to the magnetic field lines, force the coolant to follow a tortuous path. Such a system would have a larger pressure drop than if the coolant simply streamed parallel to the front face of the duct since the flow path is lengthened. Unless the ends above and below the plane of the diagram are highly curved then equation (2.10) implies that there will be no unusual flow regimes in the ducting. Misalignment of the baffles resulting in there being a component of magnetic field normal to them would radically modify the flow as shown in Fig.24b by the appearance of the shear layers parallel to the magnetic field lines. As in the cell described above, pools of stagnant fluid would be formed and the pressure gradient would increase considerably.

6. ENTRY LENGTHS

The entry length is defined as the length required for an arbitrary (e.g. turbulent) flow in a pipe entering a uniform magnetic field to become fully developed. When N is small but M is large, the entry length La is related to M and R_e in the following way

$$\begin{aligned} L &\approx R_e/M && \text{in a non-conducting duct } (\phi << M^{-1}) \\ &\approx R_e/\phi M^2 && \text{in a thin-walled duct } (M^{-1} << \phi << 1) \\ &\approx R_e/M^2 && \text{in a highly conducting walled duct } (\phi >> 1) \end{aligned} \qquad (6.1)$$

(Shercliff[37]). Thus L decreases as M increases.

However, when both M and N are very large, then, as we have seen in secs.3.1 and 3.2, the entry length either remains constant or increases as M increases, i.e.

$$\begin{aligned} L &\approx M^{\frac{1}{2}} && \text{in a non-conducting duct}^{(10,11)} \\ &\approx \phi^{-\frac{1}{2}} && \text{in a thin-walled duct}^{(10,17)} \\ &\approx 1 && \text{in a highly conducting walled duct}^{(12)} \end{aligned} \qquad (6.2)$$

Therefore, by assuming that the entry lengths derived for large and small values

of N also give the right order of magnitude for L when $N = O(1)$, it follows that we can estimate a critical Hartmann number, M_c, at which L is a minimum (L_{min}). Thus, for a non-conducting duct

$$L_{min} \approx R_c/M_c \approx M_c^{\frac{1}{2}}$$

so that $M_c \approx R_e^{2/3}$ and $L_{min} \approx R^{1/3}$. Similarly for a thin-walled duct $M_c \approx R_e^{\frac{1}{2}}\phi^{-\frac{1}{4}}$, $L_{min} \approx \phi^{-\frac{1}{2}}$ and for a highly conducting walled duct $M_c \approx R_e^{\frac{1}{2}}$ and $L_{min} \approx 1$. The M-L relationships for non-conducting and thin walled ducts are shown in Figs.25 and 26 respectively.

For a typical length of fusion reactor pipework where M and R_e are both $O(10^4)$, $M > M_c$ for either non-conducting or thin-walled pipes and the entry lengths (6.2) are appropriate.

These long distances for the flow to develop are caused by differences in the induced electric field, $\underline{v} \wedge \underline{B}$, across the duct when it changes its area or its direction relative to $\underline{B}$ or $\underline{B}$ varies along its length. If for some reason the induced electric field does not change, then the entry length is reduced.

7. DISCUSSION

During the past five years many details concerned with the simple, conceptual model of a fusion reactor discussed by Mitchell & George[38] have been studied in greater depth[33,34,35]. Allowances for MHD effects on the coolant flow have been limited to estimating the pressure drop through the blanket and associated pipework using formulae derived in Hunt & Hancox[1]. Furthermore, these estimates have been based on the assumption that the MHD flow behaves in a qualitatively similar manner to hydrodynamic flow near pipe bends, pipe area changes, etc. so that the local pressure gradient is a simple function of the local values of mean velocity and field strength perpendicular to the flow. Our present summary of MHD research studies relevant to fusion reactor technology carried out during this same period suggests that the assumed coolant flow in these reactor designs will not be realised in practice and that the pressure drop estimates may be much too low due to the effects of non-uniform fields, variable area pipework (including bends) and the formation of the very narrow shear layers.

We have already discussed some aspects of the flow in a blanket cell, namely the flow out of the inlet pipe (see sec.5.3). Carruthers[34] envisages arrays of such cells (25, divided into three adjacent rows of 8-9-8) supplied from a single feed pipe and emptying into a flat outlet header chamber which is drained by a single discharge pipe (see Fig.23a). By aligning this part of the feed pipe and the header tank parallel to the magnetic field lines he assumes that the pressure drops in those parts of the flow circuit will be negligible. Our work shows that in the header tank the flow around the mouth of each cell and the discharge pipe will be confined to thin layers of maximum thickness $O(aN^{-1/3})$ (see Fig.23b) which implies

that there will be much larger pressure gradients. However, we cannot yet say how the fluid moves between the layers on opposite walls of the tank and so the streamlines indicated in Fig.23b are only a tentative sketch of a possible flow. In the feed pipe there are numerous bends which will create large pressure drops and pressure peaks (see secs.3.1 and 3.2) and it is just conceivable that this could lead to different flow rates in each cell.

In passing from outside the magnetising coils to the blanket and back again the flow will be at right angles to the magnetic field lines (e.g. in part of the feed pipe and in the discharge pipe referred to above). An intentional overestimate of the pressure drop in these pipes has been made by calculating the pressure drop along the path of the highest magnetic field[33] and more recently a method of minimising this pressure drop by routing the pipes away from the blanket in two horizontal (but not vertical) directions rather than one has been proposed[34]. In fact the most significant pressure drop along these pipes will occur where they cross the magnetising coils and immediately upstream and downstream of them since only in such regions will the field strength gradients be large enough to give rise to the disturbed flows, pressure peaks and pressure drops discussed in sec.3.1.

At present the magnetic field strength outside of the magnetising coils is taken as zero[34] but, depending on the configuration of the coils around the toroid, there could be a significant amount of magnetic flux surrounding it to a depth equal to the minor radius of the toroid. However, before its effect on the total pressure drop can be assessed, this fringe field will have to be described in more detail.

8. ACKNOWLEDGEMENTS

Our thanks go to all the authors whose research work has contributed to this report, in particular J.S. Walker (Univ. of Illinois, U.S.A.) for his significant contributions to MHD duct flow theory.

We would also like to thank J.T.D. Mitchell and his colleagues at Culham Laboratory for their help with the work at Cambridge during the past five years.

Financial support for the work at Cambridge was received from Culham Laboratory and the Science Research Council.

Finally we gratefully acknowledge the constructive criticism by J.T.D. Mitchell and J.A. Shercliff (Univ. of Warwick) of the draft version of this report.

APPENDIX I - KULIKOVSKII's EQUATIONS[4]

The following five equations constitute the general solution of equations (2.2) which govern the effectively inviscid, inertialess core flow when $M >> 1$ and $N >> 1$

$$\underline{j}' - j_s' = B'^{-2}\underline{B}' \wedge \nabla(p'/N) \tag{AI.1}$$

$$j_s' = B' \int_o B'^{-2}\nabla(p'/N).(\underline{B}' \wedge \nabla B'^{-2})d\psi + B'P_1(\underline{A}) \tag{AI.2}$$

$$\Phi' = -\int_o\int_o^{\psi} B'^{-2}\nabla(p'/N).(\underline{B}' \wedge \nabla B'^{-2})d\psi' d\psi + \psi P_1(\underline{A}) + P_2(\underline{A}) \tag{AI.3}$$

$$\underline{v}' - v_s' = B'^{-2}\{\underline{B} \wedge \nabla\Phi' - \nabla(p'/N)\} \tag{AI.4}$$

$$v_s' = B' \int_o B'^{-2}\{B'^{-2}.\nabla^2(p'/N) + \nabla B'^{-2}.\nabla(p'/N) + \underline{B}'.(\nabla B'^{-2} \wedge \nabla\Phi')\}d\psi + B'P_3(\underline{A}) \tag{AI.5}$$

$\underline{A}$ and ψ are the magnetic vector and scalar potentials respectively, P_1, P_2 and P_3 are functions of integration with respect to ψ and the subscript s indicates the component along a magnetic field line.

APPENDIX II

In non-conducting and thin-walled ducts we have shown (sec.2.2) that to O(1)

$$\nabla\Phi' = \underline{v}' \wedge \underline{B}'$$

Now using Stokes' theorem

$$\iint (\nabla \wedge \nabla\Phi).d\underline{A}' = 0 = \int \nabla\Phi'.d\underline{\ell}$$

where $\delta\underline{\ell}$ is an elemental part of the perimeter of $\delta\underline{A}'$ (which is the cross-sectional area of a surface in the fluid). It follows, then, that

$$\int (\underline{v}' \wedge \underline{B}').d\underline{\ell} = \int (d\underline{\ell} \wedge \underline{v}').\underline{B}' = 0$$

$(\delta\underline{\ell} \wedge \underline{v}).\underline{B}$ represents the rate at which $\delta\underline{\ell}$ crosses the field lines and since there is no net gain or loss of flux enclosed by the loop then

$$\underline{B}'.\delta\underline{A}' = \text{constant}$$

Consider now a line of moving fluid particles, $\delta\underline{s}$, aligned at some given instant along a magnetic field line such that $\underline{B}' = k\delta\underline{s}$ where k is a constant. Now

$$\frac{D\underline{B}'}{D\tau} = \frac{\partial\underline{B}'}{\partial\tau} + \underline{v}'.\nabla\underline{B}' = -\nabla \wedge \underline{E}' + \underline{v}'.\nabla\underline{B}' = \nabla \wedge (\underline{v}' \wedge \nabla\underline{B}') + \underline{v}'.\nabla\underline{B}' = \underline{B}.\nabla\underline{v}$$

and

$$\frac{D}{D\tau}(k\delta\underline{s}) = k\frac{D}{Dt}(\delta\underline{s}) = k\delta\underline{v}' = k\delta\underline{s}.\nabla\underline{v}' = \underline{B}'.\nabla\underline{v}' = \frac{D\underline{B}'}{D\tau}$$

Similarly, it may be proved that the same relationship holds for higher derivatives. Hence, the line of fluid particles will continue to lie along a magnetic field line.

REFERENCES

1. HUNT, J.C.R., HANCOX, R. The use of liquid lithium as coolant in a toroidal fusion reactor. Pt.I Calculation of pumping power. UKAEA Research Group Report, Culham Laboratory, CLM-R115, 1971.
2. HANCOX, R., BOOTH, J.A. The use of liquid lithium as coolant in a toroidal fusion reactor. Pt.II Stress limitations. UKAEA Research Group Report, Culham Laboratory, CLM-R116, 1971.
3. HOFFMAN, M.A., CARLSON, G.A. Magnetic field effects in fusion reactor blankets. Proc. 1971 Intersoc. Energy Conversion Eng.Conf., Boston, Mass., Aug.3-5, pp.1096-1108.
4. SHERCLIFF, J.A. A textbook of magnetohydrodynamics. Pergamon Press Ltd., 1965.
5. ROBERTS, P.H. Singularities of Hartmann layers. Proc. Royal Soc. A 300:94, 1967.
6. KULIKOVSKII, A.G. On slow steady flows of conductive fluid with high Hartmann number. Izv.Akad.Nauk SSSR, Mekh.Zhid. i Gaza, 3:2:3, 1968.
7. HUNT, J.C.R., LUDFORD, G.S.S. Three-dimensional MHD duct flows with strong transverse magnetic fields. Pt.I Obstacles in a constant area duct. J. Fluid Mech., 33:693, 1968.
8. WALKER, J.S., LUDFORD, G.S.S., HUNT, J.C.R. Three dimensional MHD duct flows with strong transverse magnetic fields. Pt.III Variable area rectangular ducts with insulating walls. J. Fluid Mech., 56:121, 1972.
9. KULIKOVSKII, A.G. Flows of a conducting incompressible liquid in an arbitrary region with a strong magnetic field. Izv.Akad.Nauk SSSR, Mekh.Zhid. i Gaza, 8:3:144, 1973.
10. HOLROYD, R.J., WALKER, J.S. A theoretical study of the effects of wall conductivity, non-uniform magnetic fields and variable area ducts on liquid metal flows at high Hartmann number. J.Fluid Mech. Vol 84 1978
11. WALKER, J.S., LUDFORD, G.S.S. MHD flow in insulated circular expansions with strong transverse magnetic fields. Int.J.Eng.Sci., 12:12:1045, 1974.
12. WALKER, J.S., LUDFORD, G.S.S. MHD flow in conducting circular expansions with strong transverse magnetic fields. Int.J.Eng.Sci., 12:3:193, 1974.
13. WALKER, J.S., LUDFORD, G.S.S. MHD flow in variable area conducting rectangular ducts. Proc. 13th Midwestern Mech.Conf., Developments in Mechanics, 7:265, 1973.
14. HUNT, J.C.R., LEIBOVICH, S. MHD flow in channels of variable cross-section with strong transverse magnetic fields. J. Fluid Mech., 28:241, 1967.
15. HUNT, J.C.R., SHERCLIFF, J.A. MHD at high Hartmann number. Ann.Rev. Fluid Mech., 3:37, 1971.
16. SHERCLIFF, J.A. The flow of conducting fluids in circular pipes under transverse magnetic fields. J. Fluid Mech., 1:644, 1956.
17. WALKER, J.S., LUDFORD, G.S.S. MHD flow in circular expansions with thin

conducting walls. Int.J.Eng.Sci., 13:3:261, 1975.

18. YOUNG, F.J., HOLCOMB, R.J., FRAAS, A.P. MHD test of a one-sixth scale model of a CTR recirculating lithium blanket. Oak Ridge National Lab. Report ORNL TM 4818, 1975.
19. HOLROYD, R.J. MHD duct flows in non-uniform magnetic fields. Ph.D. dissertation, Univ. of Cambridge, 1976.
20. BRANOVER, G.G., SHCHERBININ, E.V. MHD jet flow in a bounded space. Mag.Gidro., 2:3:5, 1966.
21. SLYUSAREV, N.M., SHILOVA, E.I., SHCHERBININ, E.V. Experimental study of MHD flows in converging and diverging channels. Mag.Gidro., 6:4:59, 1970.
22. HOLROYD, R.J. Some thoughts about liquid metal MHD flow in a rectangular duct with mixed wall conductivities. Submitted for publication in J. Fluid Mech. (1977).
23. ALTY, C.J.N. MHD duct flow in uniform transverse magnetic fields at arbitrary orientation. J. Fluid Mech., 48:429, 1971.
24. HUNT, J.C.R. Some aspects of magnetohydrodynamics. Ph.D. dissertation, Univ. of Cambridge, 1967.
25. HUNT, J.C.R., MALCOLM, D.G. Some electrically driven flows in MHD. Pt.II Theory and experiment. J. Fluid Mech., 33:775, 1968.
26. MALCOLM, D.G. Investigation of a steady MHD shear layer using hot film anemometry. Nature 224:909, 1969.
27. GLABERSON, W.I., DONNELLY, R.J., ROBERTS, P.H. Hydromagnetic duct flow: theory and experiment. Physics of Fluids, 11:2192, 1968.
28. CHANG, C.-C., LUNDGREN, T.S. Duct flow in MHD. Zeit.angew.Math.Phys., 12:100, 1961.
29. BRANOVER, H. On some important effects in laboratory MHD flows in rectangular ducts in transverse magnetic fields. Proc. 14th Symp.Eng. Aspects of MHD, Univ. of Tennessee Space Institute, April 1974.
30. BOCHENINSKII, V.P., BRANOVER, G.G., TANANAEV, A.V., CHERNYAEV, Yu.P. Experimental investigation of the resistance to the flow of a conducting fluid in flat insulated ducts in the presence of a transverse magnetic field with allowance for fringe effects and wall roughness. Izv.Akad.Nauk SSSR, Mekh.Zhid. i Gaza, 6:4:10, 1971.
31. CARLSON, G.A. MHD pressure drop of lithium flowing in conducting wall pipe in a transverse magnetic field - theory and experiment. UCRL-75307, Lawrence Livermore Laboratory, April 1974.
32. TEMPERLEY, D.J., TODD, L. The effect of wall conductivity in MHD duct flows at high Hartmann number. Proc. Cambridge Phil.Soc., 69:337, 1971.
33. STANBRIDGE, J.R., CARRUTHERS, H.M., KEEN, B.A., SHOTTER, H.A. Design of stainless steel blanket cells for a fusion reactor. UKAEA Research Group Report,

Culham Laboratory, CLM-R127, 1974.

34. CARRUTHERS, H.M. Structural design of demountable blanket elements and shield for a fusion reactor. UKAEA Research Group Report, Culham Laboratory, CLM-R151, 1976.

35. STANBRIDGE, J.R., SHOTTER, H.A. Review of irradiation creep and swelling in a fusion reactor blanket cell structure. UKAEA Research Group Report, Culham Laboratory, CLM-R152, 1976.

36. BADGER, B. et al. UWMAK-I. A Wisconsin toroidal fusion reactor design. Univ. of Wisconsin Report UWFDM-68, March 1974.

37. SHERCLIFF, J.A. The theory of electromagnetic flow measurement. Cambridge University Press, 1962.

38. MITCHELL, J.T.D., GEORGE, M.W. A design concept for a fusion reactor blanket and magnetic shield structure. UKAEA Research Group Report, Culham Laboratory, CLM-R121, 1972.

NOTATION

Vector quantities

Physical quantity	Dimensionless quantity	
	$\underline{A}$	magnetic vector potential
$\underline{B}$	$\underline{B}'$	magnetic field
$\underline{E}$	$\underline{E}'$	electric field
$\underline{j}$	$\underline{j}'$	electric current density
	$\underline{j}'_\infty$	value of core variable $\underline{j}'$ at duct wall
	$\underline{n}'$	co-ordinate normal to wall into fluid
	$\hat{n}$	unit vector parallel to $\underline{n}'$
$\underline{v}$	$\underline{v}'$	velocity
	$\underline{v}'_\infty$	value of core variable $\underline{v}'$ at duct wall
$\underline{x}$	$\underline{x}'$	position vector with components x,y,z
	$\delta\underline{A}'$	elemental area in fluid
	$\delta\underline{\ell}$	elemental part of perimeter of $\delta\underline{A}'$

Scalar quantities

Physical quantity	Dimensionless quantity	
	A'_o	total area of conducting walls in rectangular duct
a		hydraulic radius (general), radius of circular duct, semi-height of rectangular duct (i.e. parallel to $\underline{B}$)
B_o		reference value of flux density
b		semi-width of rectangular duct
$d\bar{p}/dz$		extra pressure gradient due to circulating current
$(dp/dy)_{//}$		pressure gradient of flow in pipe aligned with uniform magnetic field
$(dp/dy)_v$		pressure gradient of hydrodynamic flow
	E_o	equivalent to E'_x in rectangular duct analysis
	f_1	$(1-x^2)^{\frac{1}{2}} + (r^2-x^2)^{\frac{1}{2}}$
	f_2	$\phi(1-x^2)^{\frac{1}{2}} + \phi_r(r^2-x^2)^{\frac{1}{2}}$
	$g(x',z')$	arbitrary function of integration
	I	value of integral $\int_o^{S_o} ds/B$ along a field line
	k	numerical constant
La	L	entry length
	L_{min}	minimum value of L
ℓa	ℓ	length over which a fully-developed flow is disturbed
	m	$(\phi b)^{-\frac{1}{2}}$
	$P(\underline{A})$	P_1, P_2, P_3 arbitrary functions of integration
p	p'	pressure

Q		volumetric flow rate
R		radius of bend in pipe
	r	radius of pipe (or rod) inside a duct
	S_o	total length of field line inside duct
	s	distance measured along a field line
t		thickness of duct wall
v_o		mean velocity of flow
	$Y(\underline{x}')$	duct wall
	α	fractional decrease in field strength
Δp		net pressure drop due to circulating current
$\Delta\bar{p}$		extra pressure rise or fall due to $d\bar{p}/dz$
$\Delta\Phi$		potential difference across duct
δ		thickness of shear layer
	ε	$\{(\kappa+1)/(\kappa-1)\}^{\frac{1}{2}}$
	ζ	co-ordinate normal to shear layer and $\underline{B}$
η		viscosity
	Θ	velocity stream function
	θ	semi-apex angle in diamond shaped duct
	κ	$M\phi$
λa	λ	extent of non-uniform magnetic field
μ		magnetic permeability (of free space)
	ξ	$\tan(\frac{1}{2}\sin^{-1}r)$
ρ		density
σ		electrical conductivity of fluid
σ_w		electrical conductivity of duct wall
τ	τ'	time
Φ	Φ'	electric potential
	Φ'_w	electric potential in duct wall
	Φ'_∞	value of core variable Φ' at duct wall
	ψ	magnetic scalar potential

Dimensionless groups

M	Hartmann number	$aB_o\sqrt{\sigma/\eta}$
N	interaction parameter	$\sigma B_o^2 a/\rho v_o = M^2/R_e$
R_e	Reynolds number	$av_o\rho/\eta$
R_m	magnetic Reynolds number	$\sigma\mu av_o$
ϕ	conductance ratio	$\sigma_w t/\sigma a$

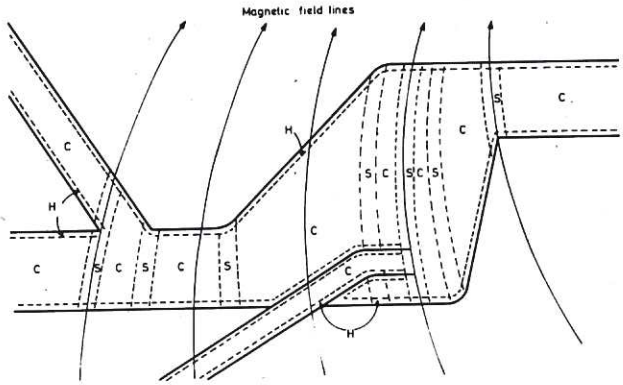

Fig.1a Prototype ducting showing regions for analysing flow when M, N, $R_e \gg 1$
C. core
H. Hartmann layers
S. shear layers.

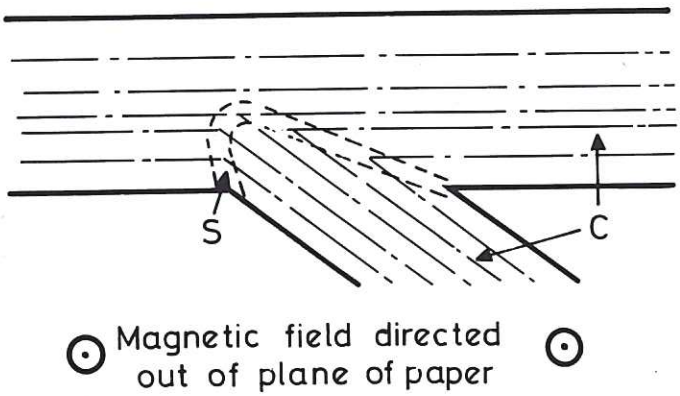

Fig.1b Plan view of 'characteristic surfaces' (- ——-) near a junction of two pipes in above duct showing how shear layers (S) are located. C indicates core flow.

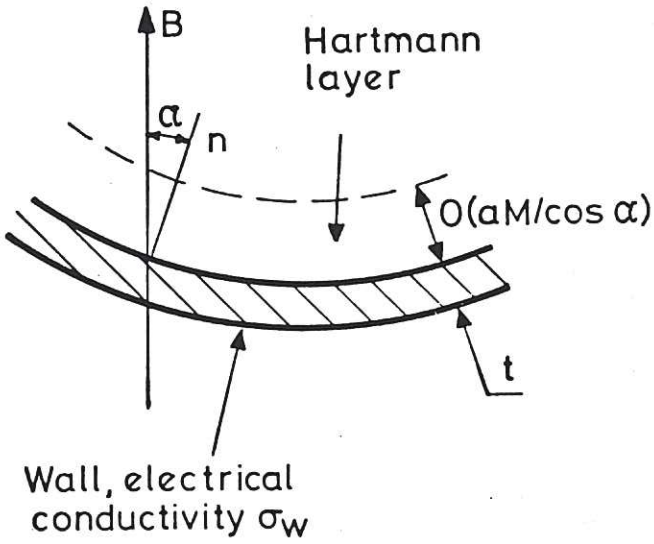

Fig.2 Notation for analysis of Hartmann layer.

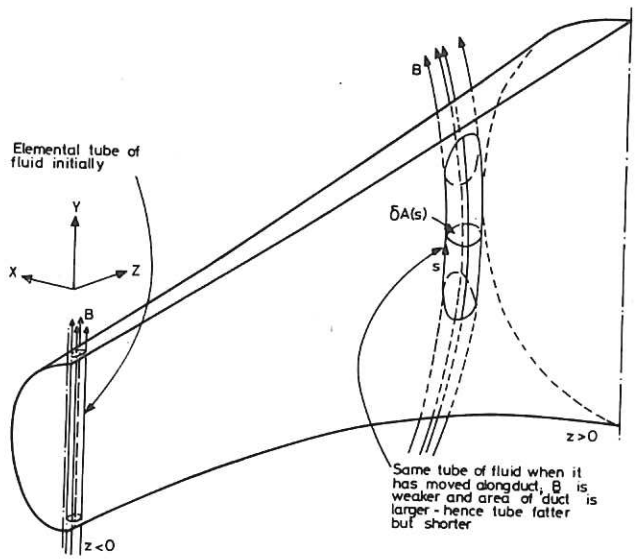

Fig.3 Elemental tube of fluid moving along duct such that (i) it always contains the same volume of fluid, (ii) its cross-section always encloses the same amount of magnetic flux, (iii) its surface generators are magnetic field lines.

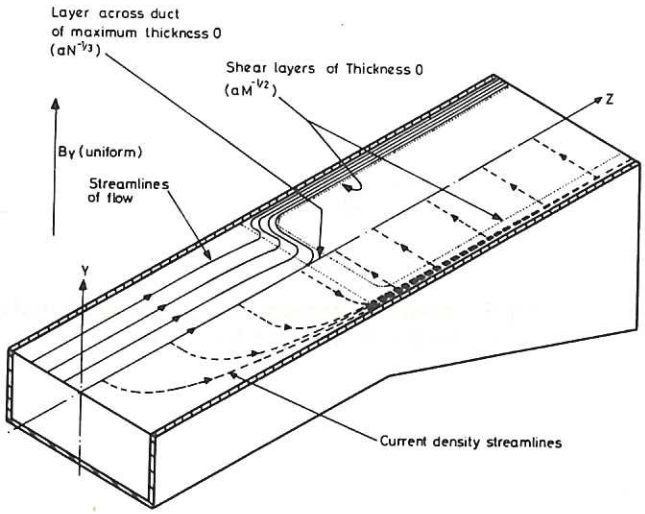

Fig.4a Streamlines of flow and current flow on centre plane in a rectangular duct with $\phi \ll 1$ and increasing cross-section.

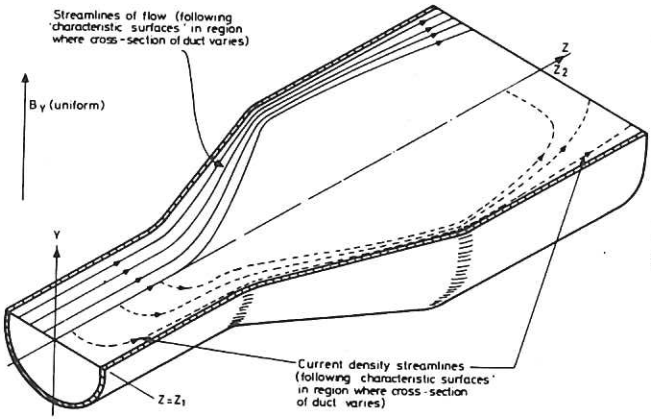

Fig.4b Streamlines of flow and current flow on centre plane in a circular duct with $\phi \ll 1$ and increasing cross-section.

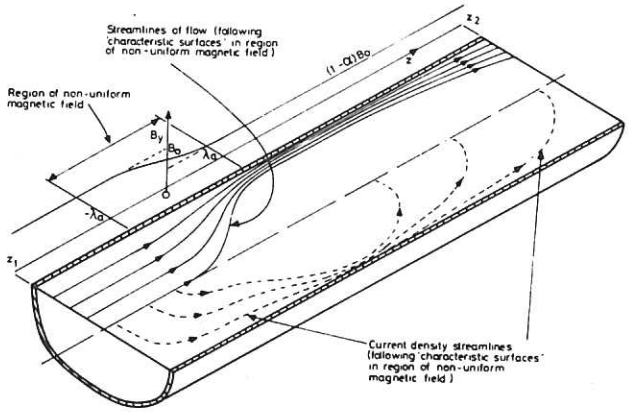

Fig.4c Streamlines of flow and current flow on centre plane in a uniform bore circular duct with $\phi \ll 1$ when the field strength decreases.

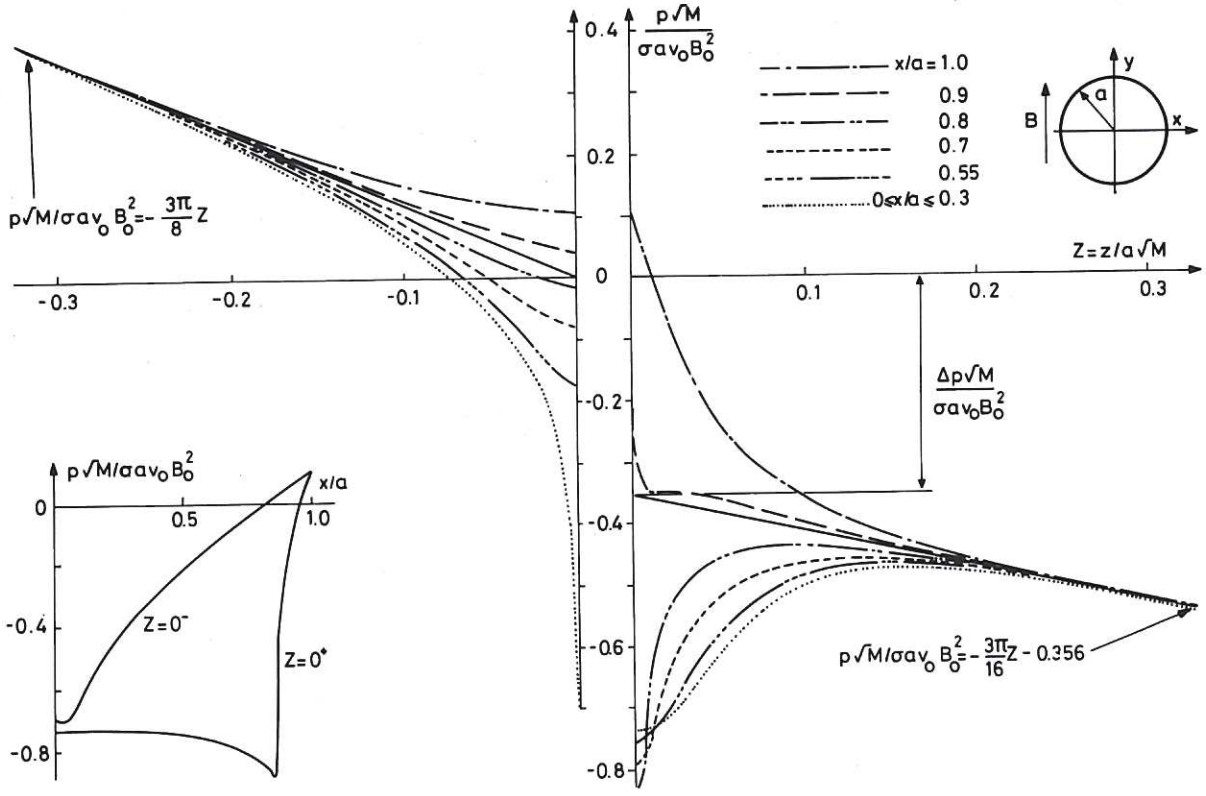

Fig.5 Theoretical pressure distribution along uniform bore, circular, non-conducting duct when $B_y = 1$ for $Z < 0$, $B_y = 0.5$ for $Z > 0$.

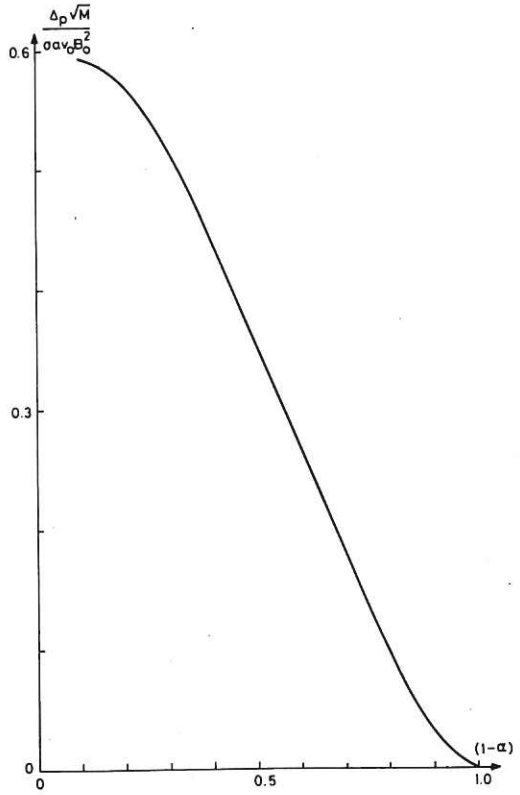

Fig.6 Variation of pressure drop Δp defined in Fig.5 with reduction in flux density ($1-a = B_y(Z > 0)/B_0$).

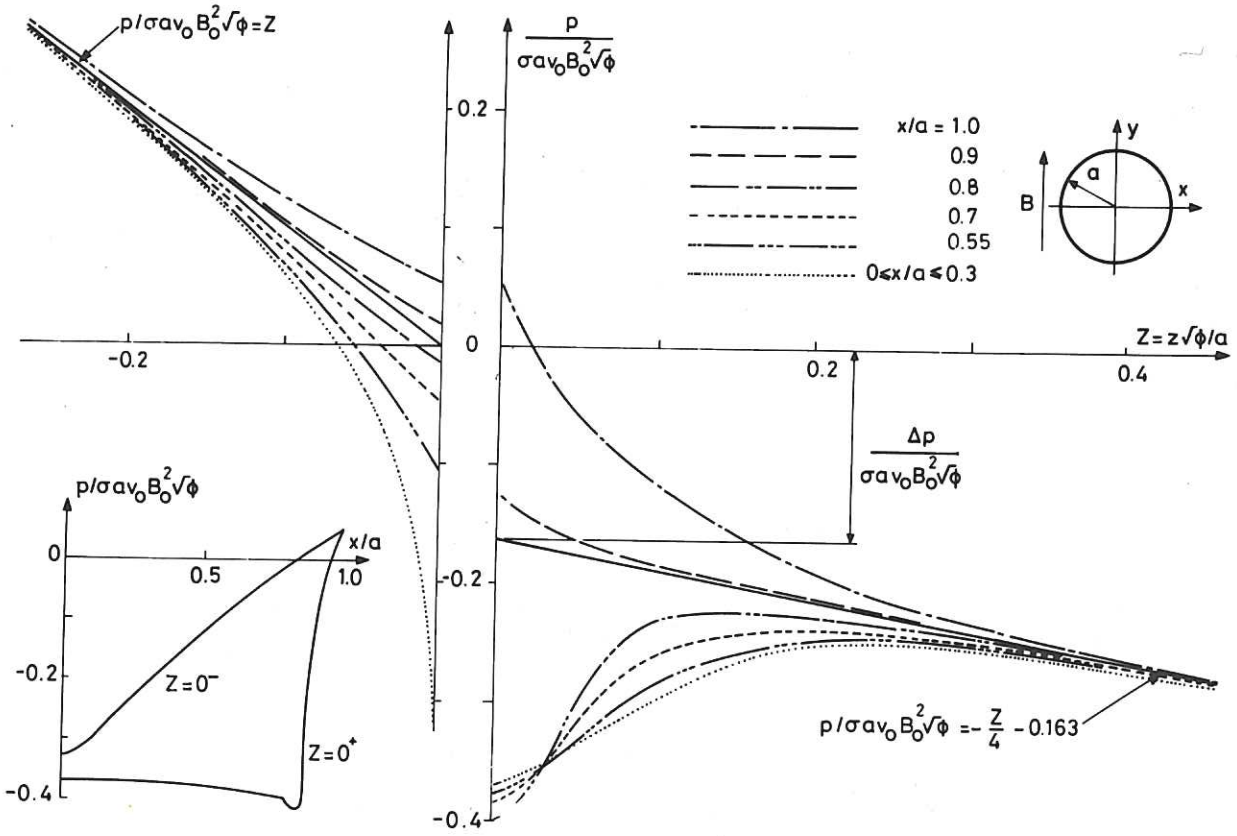

Fig.7 Theoretical pressure distribution along uniform bore, circular, thin-walled duct ($M^{-1} \ll \phi^{1/2} \ll 1$) when $B_y = 1$ for $Z < 0$, $B_y = 0.5$ for $Z > 0$.

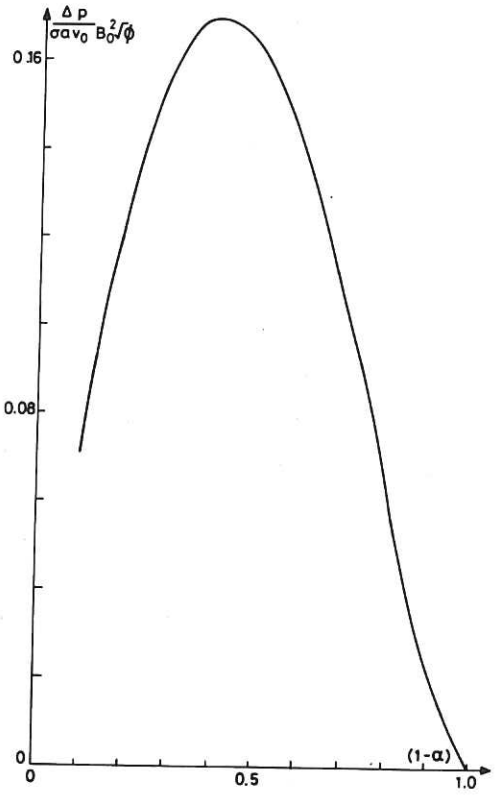

Fig.8 Variation of pressure drop Δp defined in Fig.7 with reducation in flux density ($1-a = B_y(Z > 0)/B_0$).

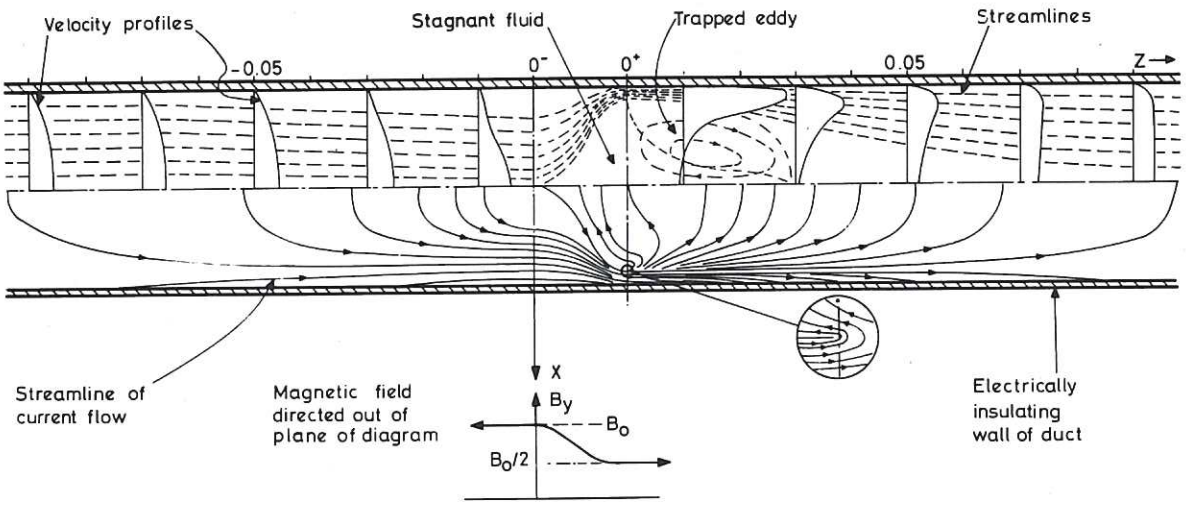

Fig.9 Theoretical streamlines, velocity profiles and current streamlines on centre plane in a uniform bore, circular, non-conducting duct, when the field strength decreases.

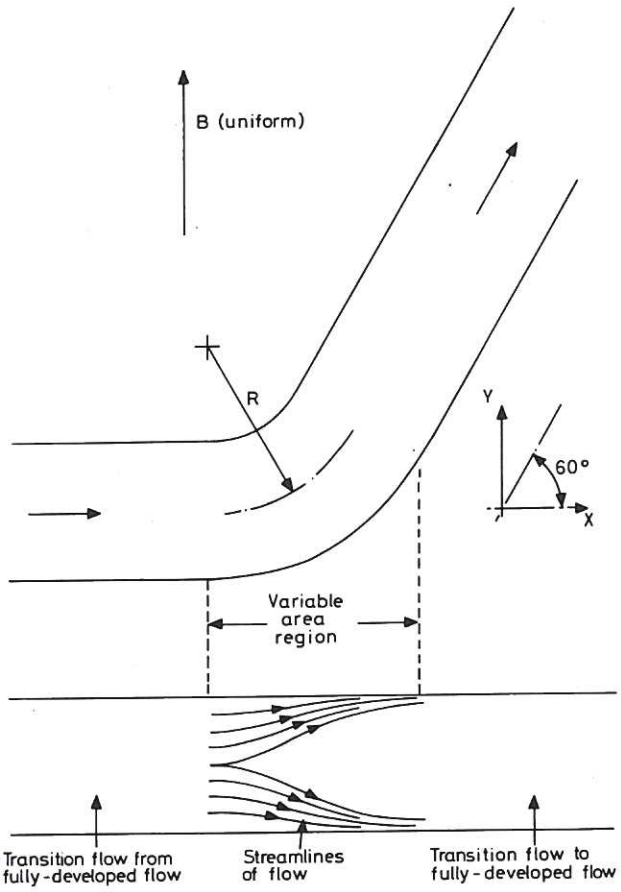

Fig.10 Bend in non-conducting or thin-walled pipe in the plane of a uniform magnetic field. Plan view shows effect on streamlines of flow in vicinity of bend.

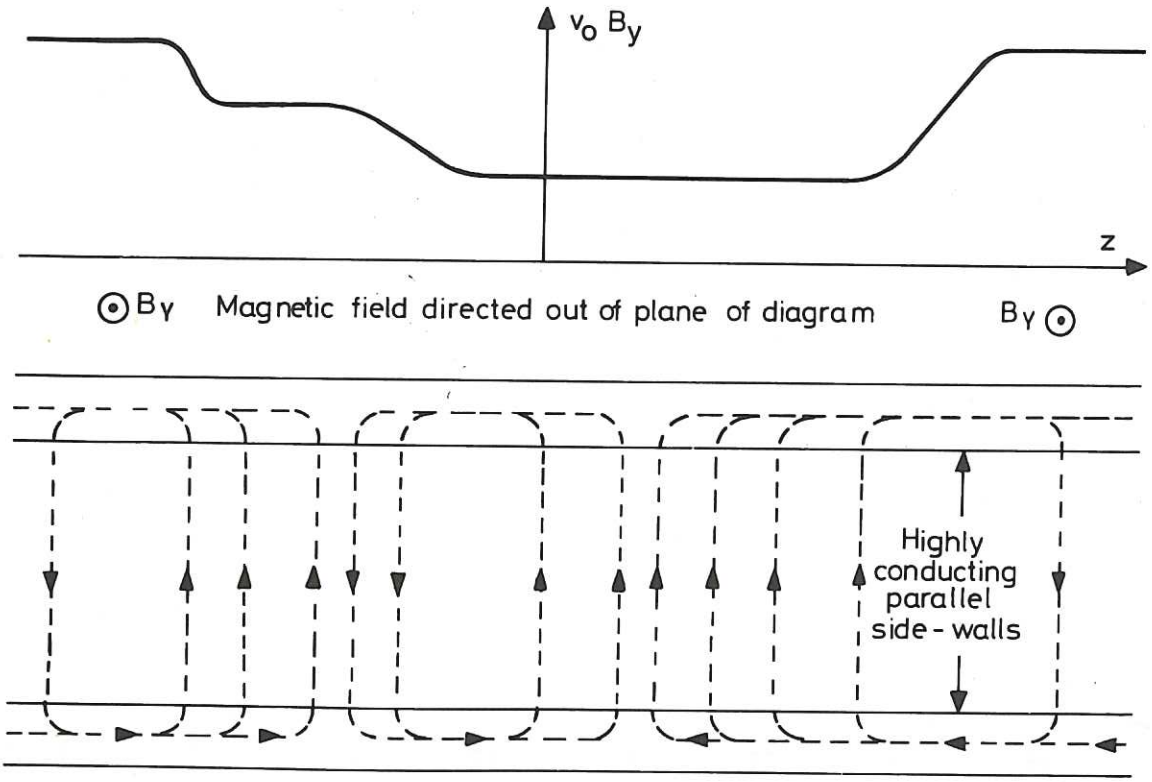

Fig.11 Recirculating electric currents (- - -) due to variations in induced electric field $v_o B_y$ in a rectangular duct with very highly conducting walls ($\phi \to \infty$) parallel to magnetic field lines and non-conducting walls top and bottom which may diverge. Changes in $v_o B_y$ may be caused by changes in $\underline{B}$ or area of duct (and hence v_o).

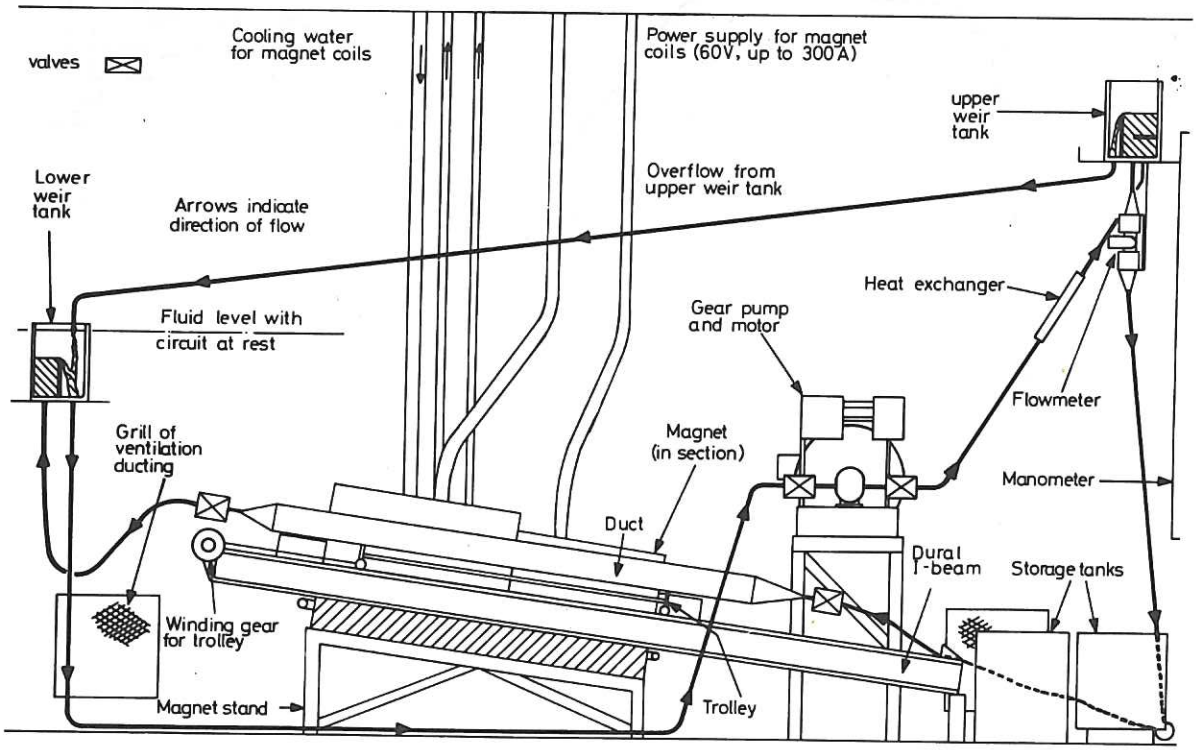

Fig.12 Elevation of rig built for experiments at Cambridge. The electromagnet is sectioned to show duct and duct supporting grear. Weir tanks are sectioned to show how they maintain a constant pressure difference across circuit and hence constant flow rate through the duct.

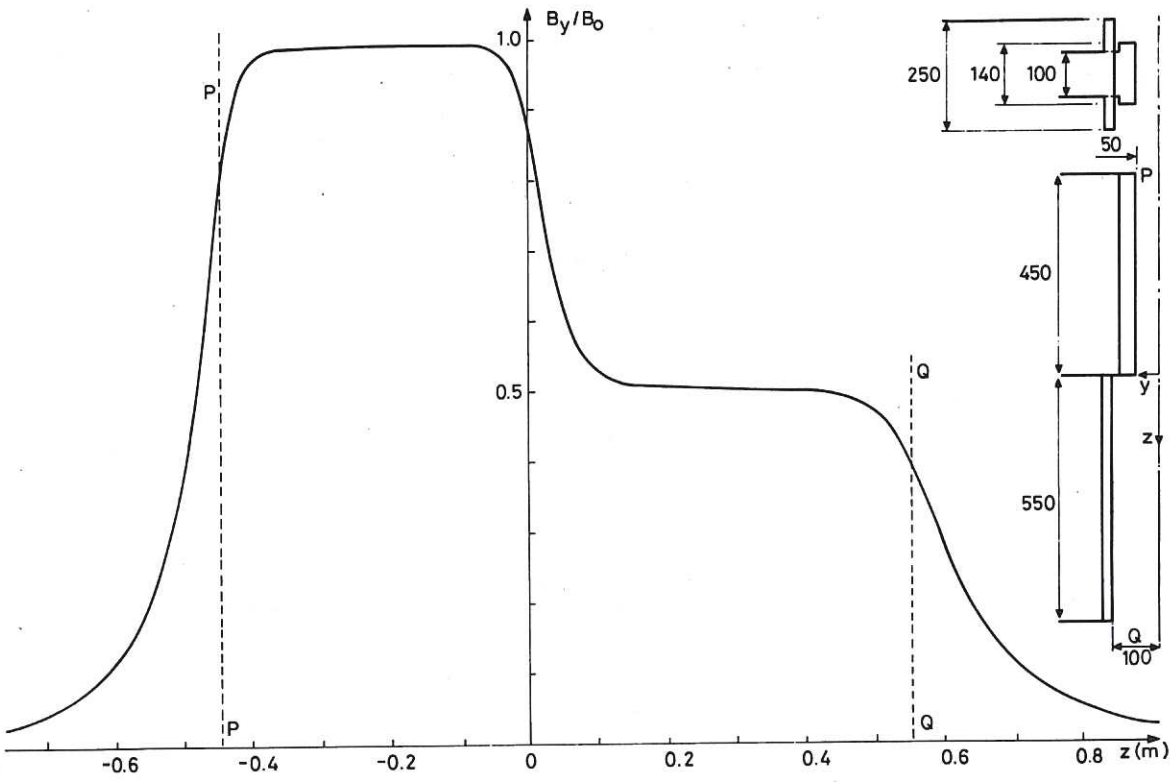

Fig.13a Step-change field – variations of B_y along centre-line of air gap. End elevation and plan half-views of pole pieces shown on right with principal dimensions in mm.

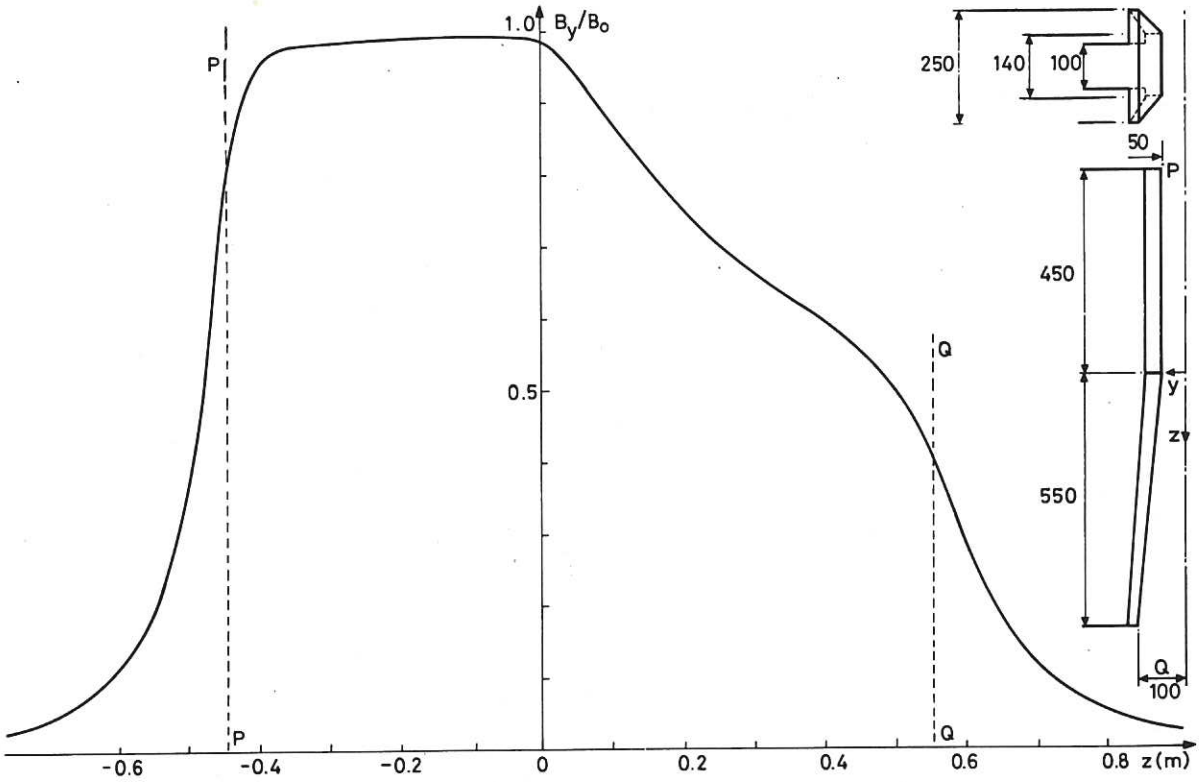

Fig.13b Slow change field – variation of B_y along centre-line of air gap. End elevation and plan half-views of pole pieces shown on right with principal dimensions in mm.

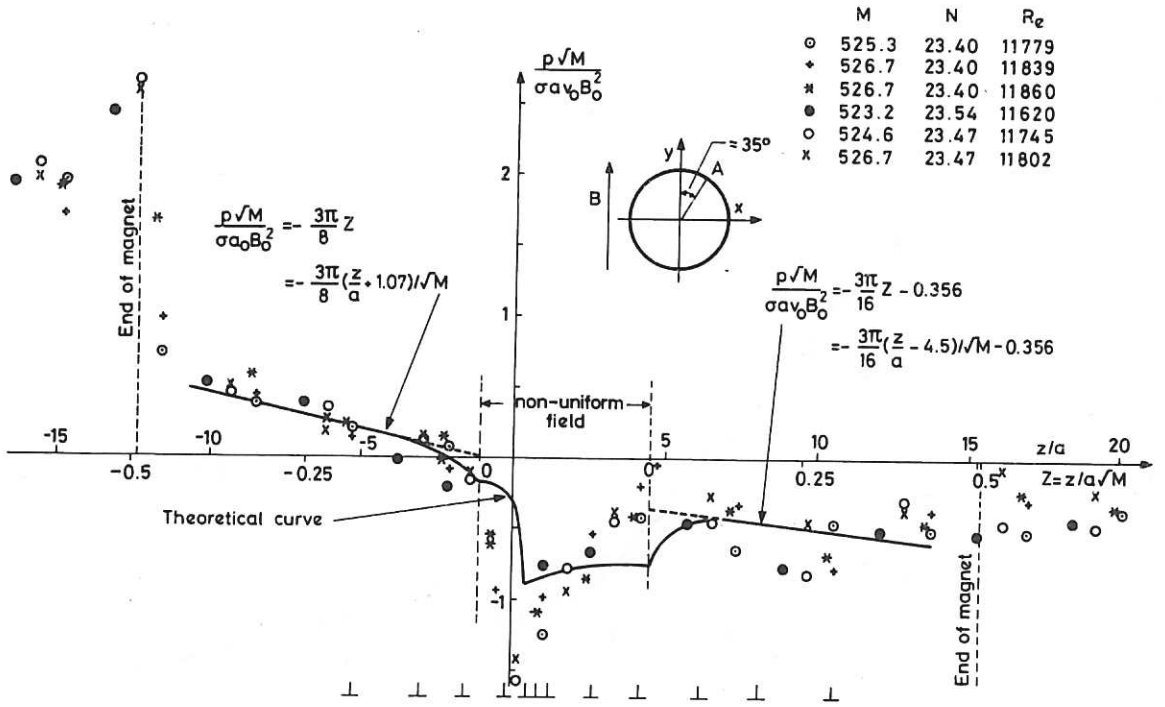

Fig.14 Pressure distribution along non-conducting duct at A for step-change field (Fig.13a) (theory and experiment). (⊥ symbols referred to in Fig.15.)

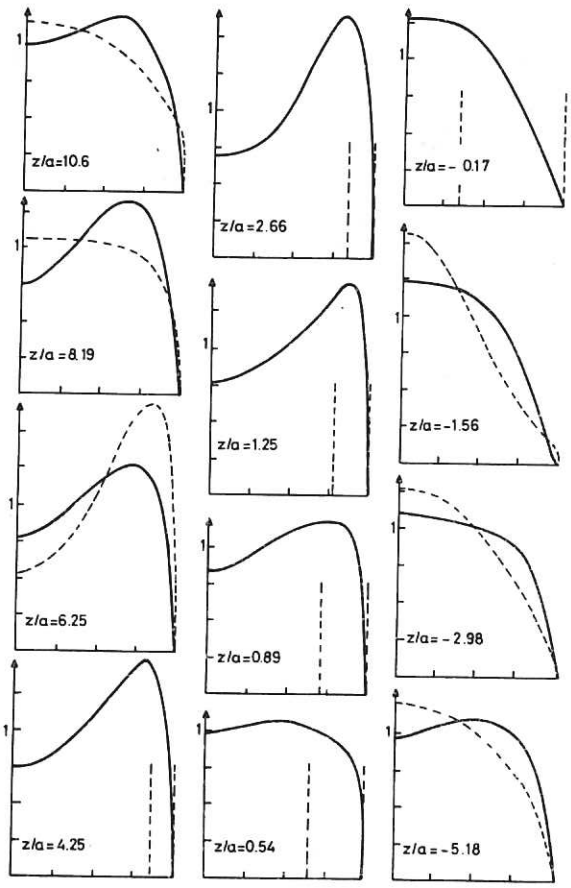

Fig.15 Velocity profiles of v_x/v_o across non-conducting duct on centre plane for step-change field (Fig.13a). - - - theory, —— experiment (from potential and hot film probe readings). Over the range $4.25 \geqslant z/a \geqslant -0.17$ the exact theoretical profile cannot be determined but the flow is confined to that part of the duct between the vertical dashed lines with arrow heads. Positions of profiles are indicated by ⊥ in Fig.14.

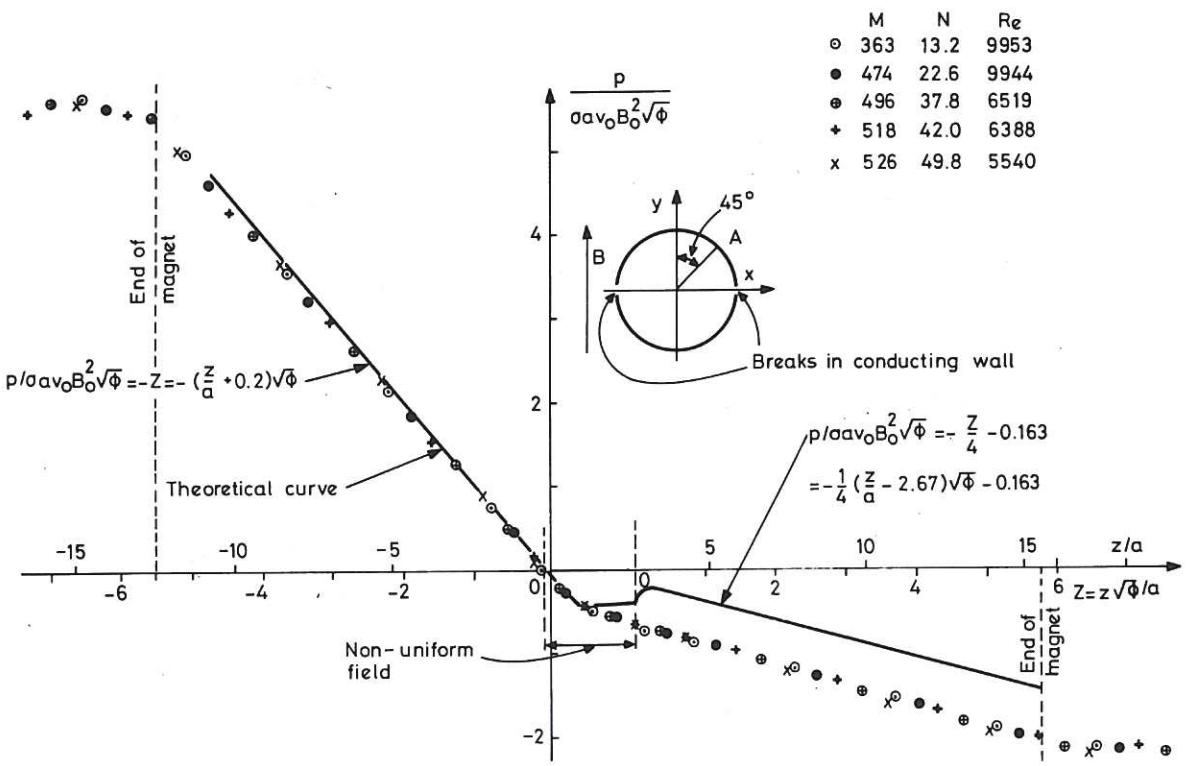

Fig.16 Pressure distribution along thin-walled duct at A for step-change field (Fig.13a) (theory and experiment).

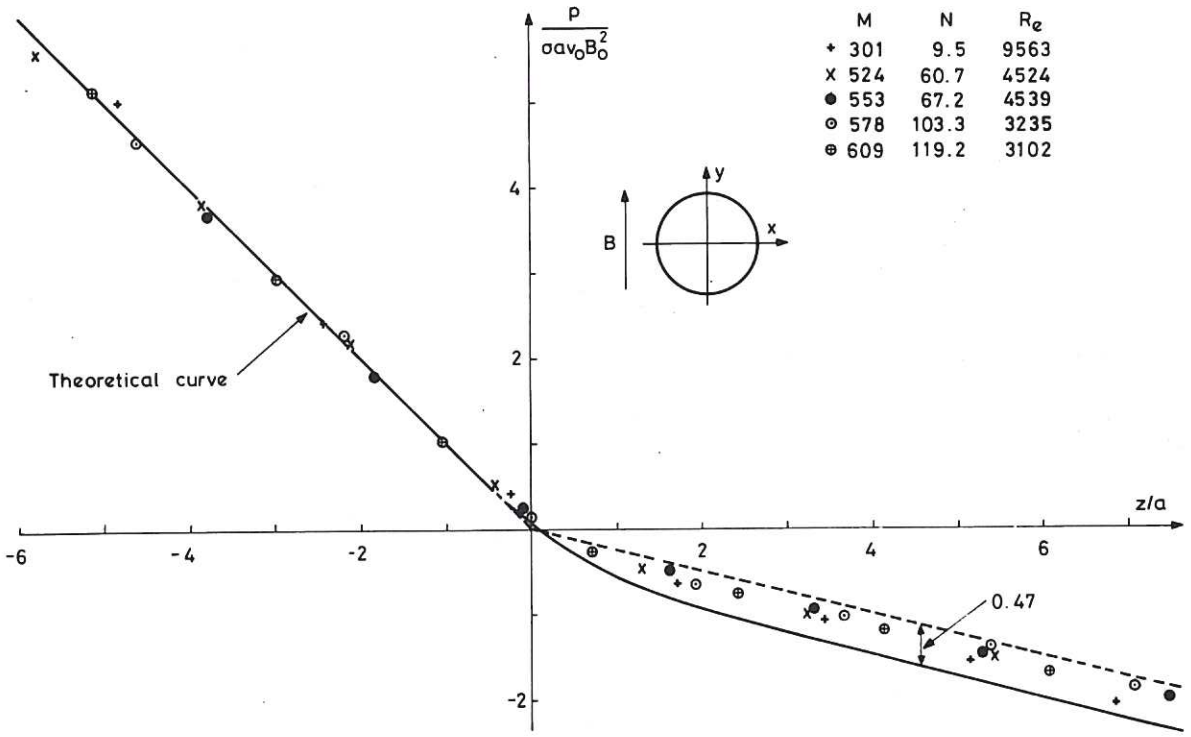

Fig.17 Pressure distribution along highly-conducting walled duct, $\phi = 8.75$ for step-change field (Fig.13a) (theory and experiment).

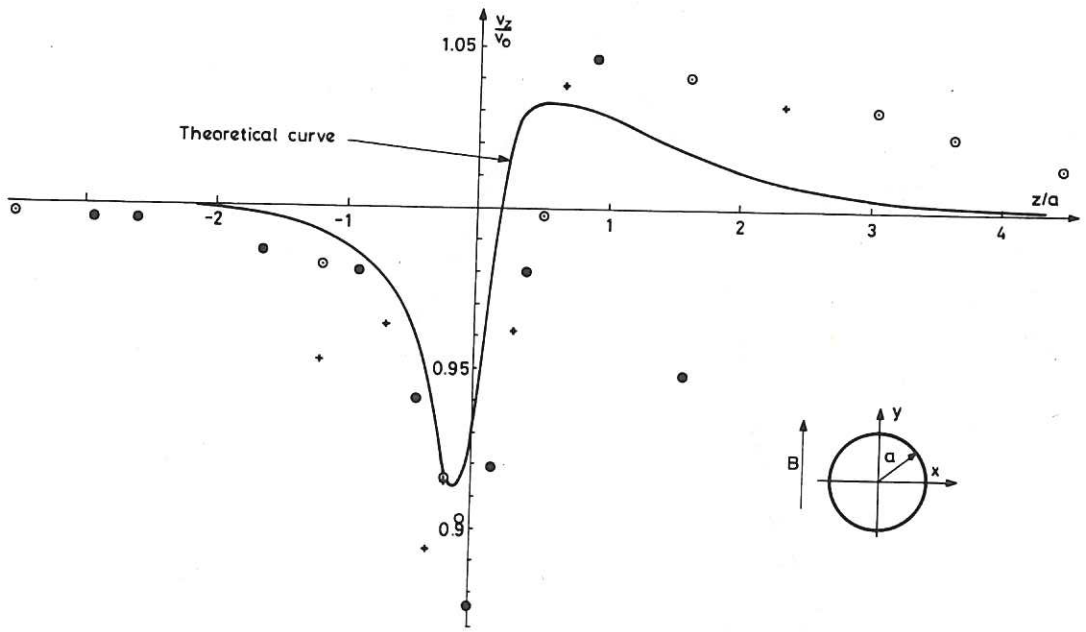

Fig.18 Velocity distribution along highly-conducting walled duct at x/a = 0, y/a = 0.86 for step-change field (Fig.13a) (theory and experiment). Different symbols represent separate sets of measurements but all with M = 603, N = 96.7, R_e = 3765.

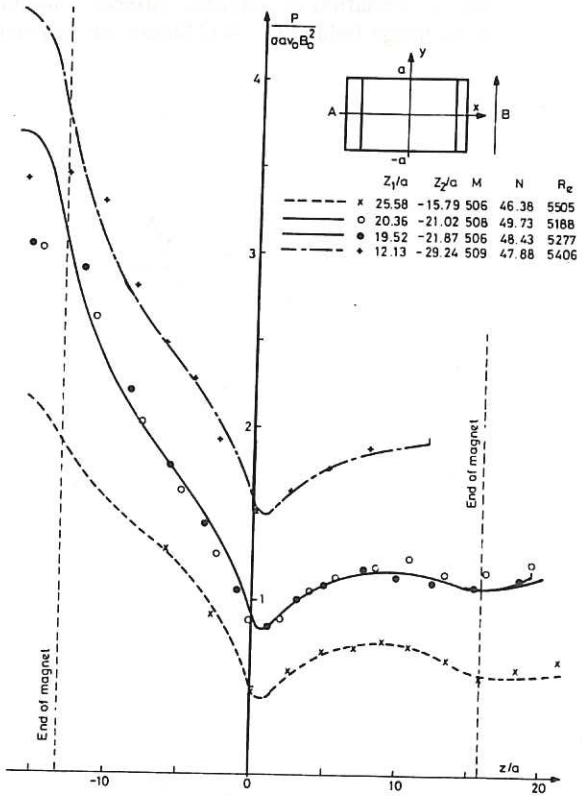

Fig.19 Pressure distribution along rectangular duct at A for step-change field (Fig.13a). Z_1 and Z_2 represent the positions of the downstream and upstream ends of the conducting walls respectively (theory and experiment).

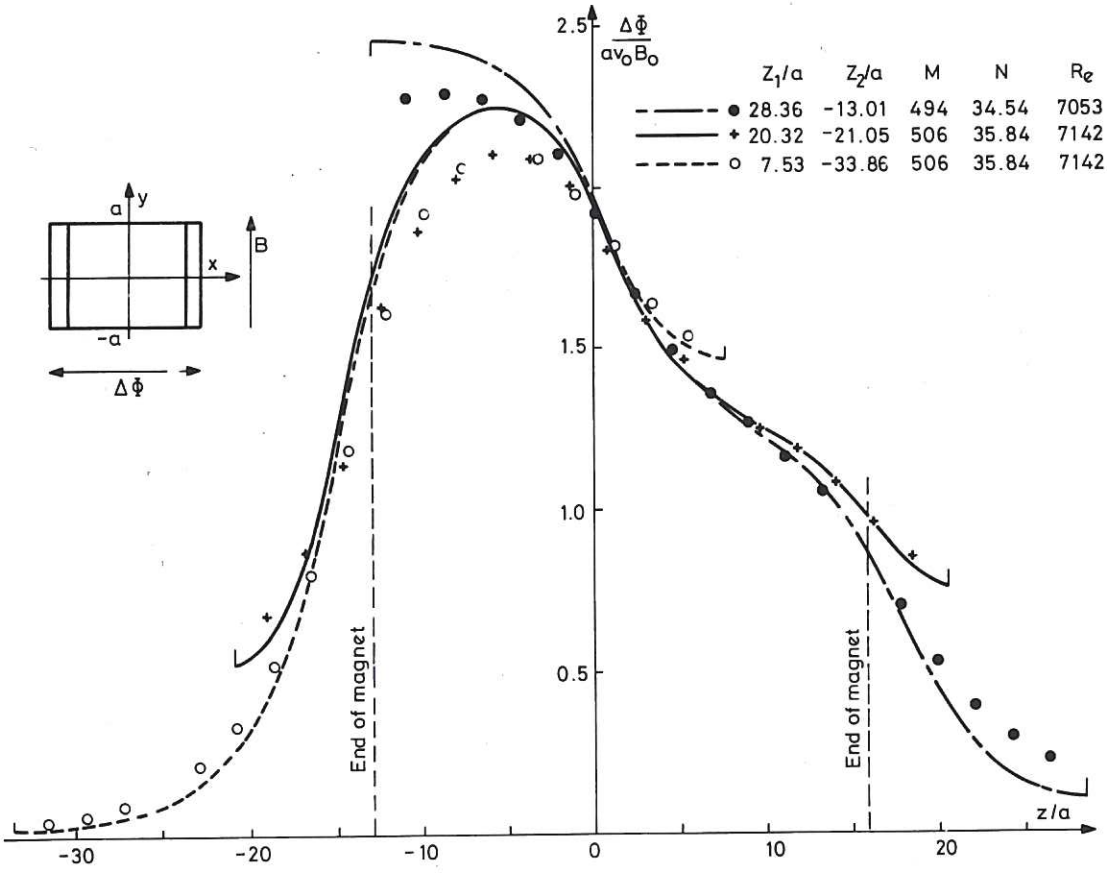

Fig.20 Variation of potential difference between conducting walls, $\Delta\Phi$, along rectangular duct for step-change field (Fig.13a) (theory and experiment).

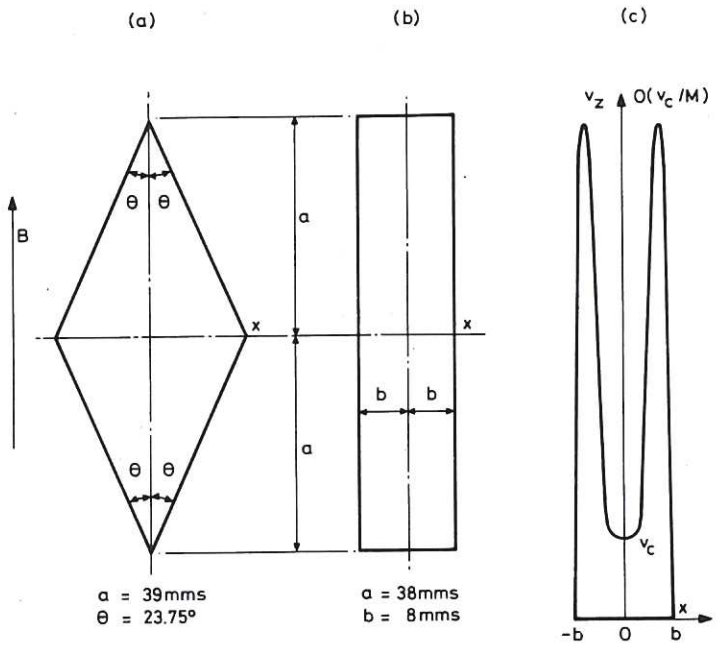

Fig.21a. Thin-walled diamond shaped duct with dimensions. Fig.21b. Thin-walled slim rectangular duct with dimensions. Fig.21c. Typical velocity profile across slim rectangular duct.

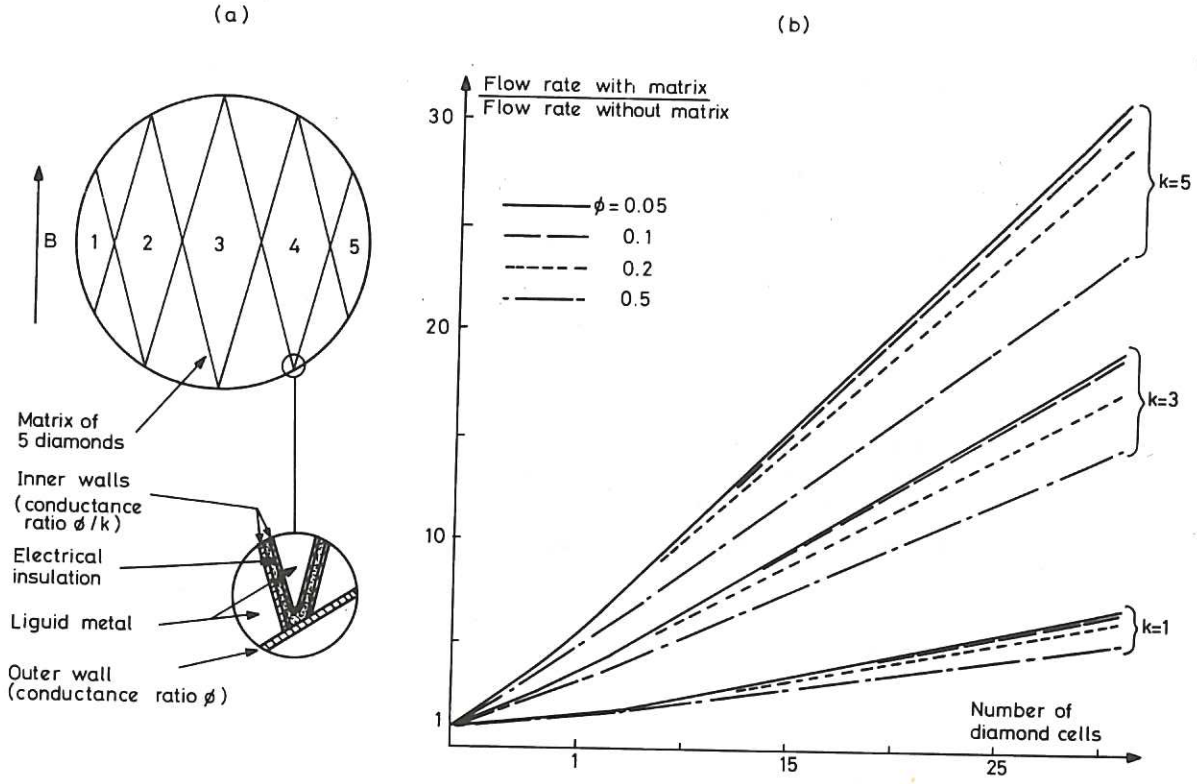

Fig.22a. Matrix of 5 diamond cells inserted in a circular pipe. Fig.22b. Increase in flow rate due to matrix of diamond cells.

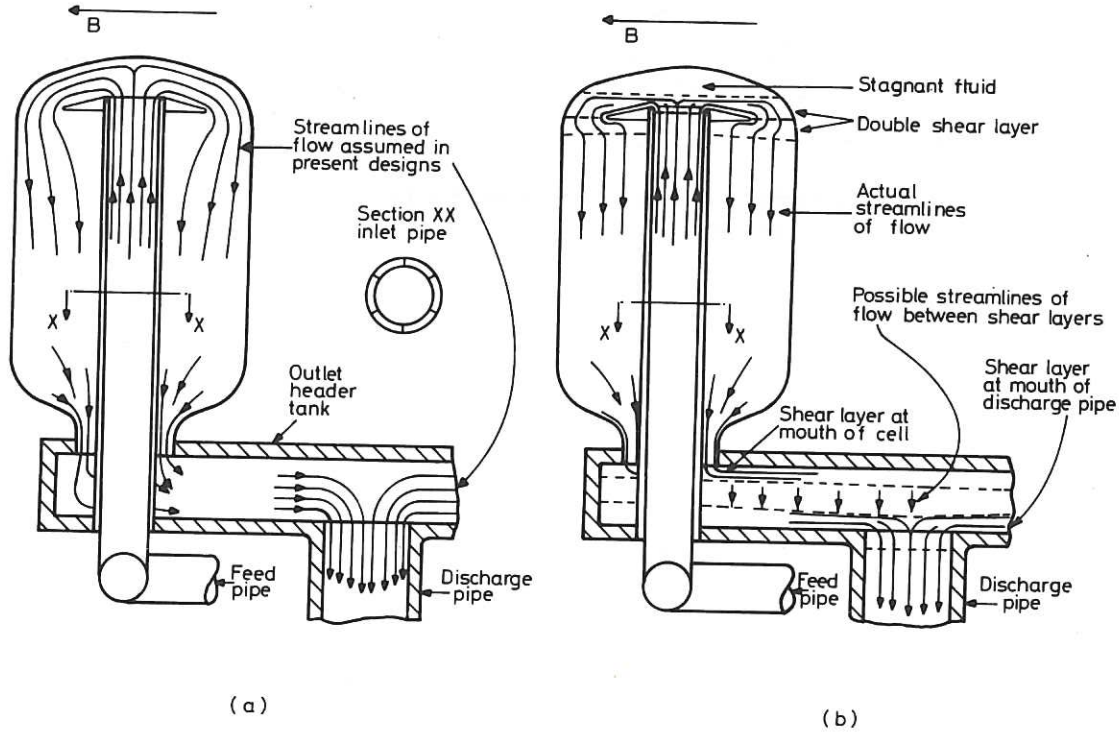

Fig.23a Required motion of liquid metal coolant in blanket cell (arrows indicate streamlines of flow).
Fig.23b Actual flow of coolant in blanket cell caused by MHD effects.

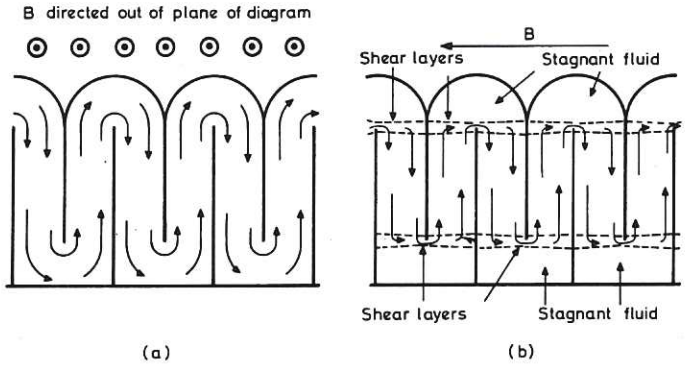

Fig.24a Zig-zag path of coolant in blanket proposed in research studies at University of Wisconsin. Magnetic field lines are parallel to thin metal baffles.

Fig.24b Effect of misalignment of magnetic field and baffles.

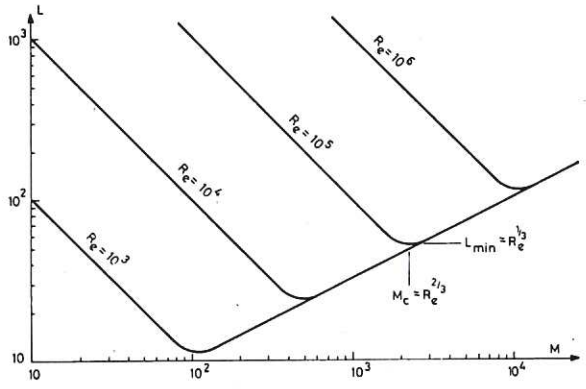

Fig.25 Variation of entry length L with M and R_e in a non-conducting duct.

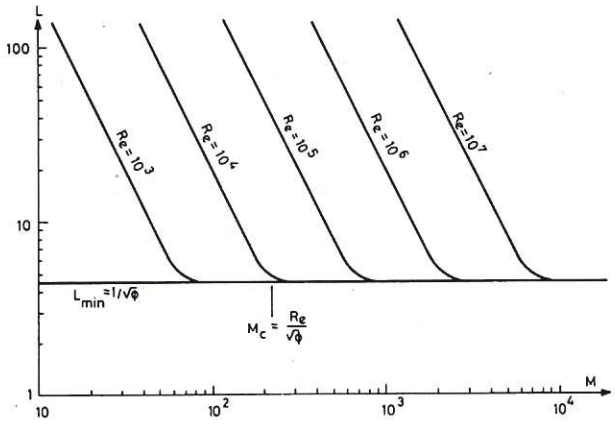

Fig.26 Variation of entry length L with M and R_e in a thin-walled duct.

HER MAJESTY'S STATIONERY OFFICE

Government Bookshops

49 High Holborn, London WC1V 6HB
13a Castle Street, Edinburgh EH2 3AR
41 The Hayes, Cardiff CF1 1JW
Brazennose Street, Manchester M60 8AS
Wine Street, Bristol BS1 2BQ
258 Broad Street, Birmingham B1 2HE
80 Chichester Street, Belfast BT1 4JY

Government publications are also available through booksellers